Control of a three-port converter for human power

R.C.T. Wilmer BSc

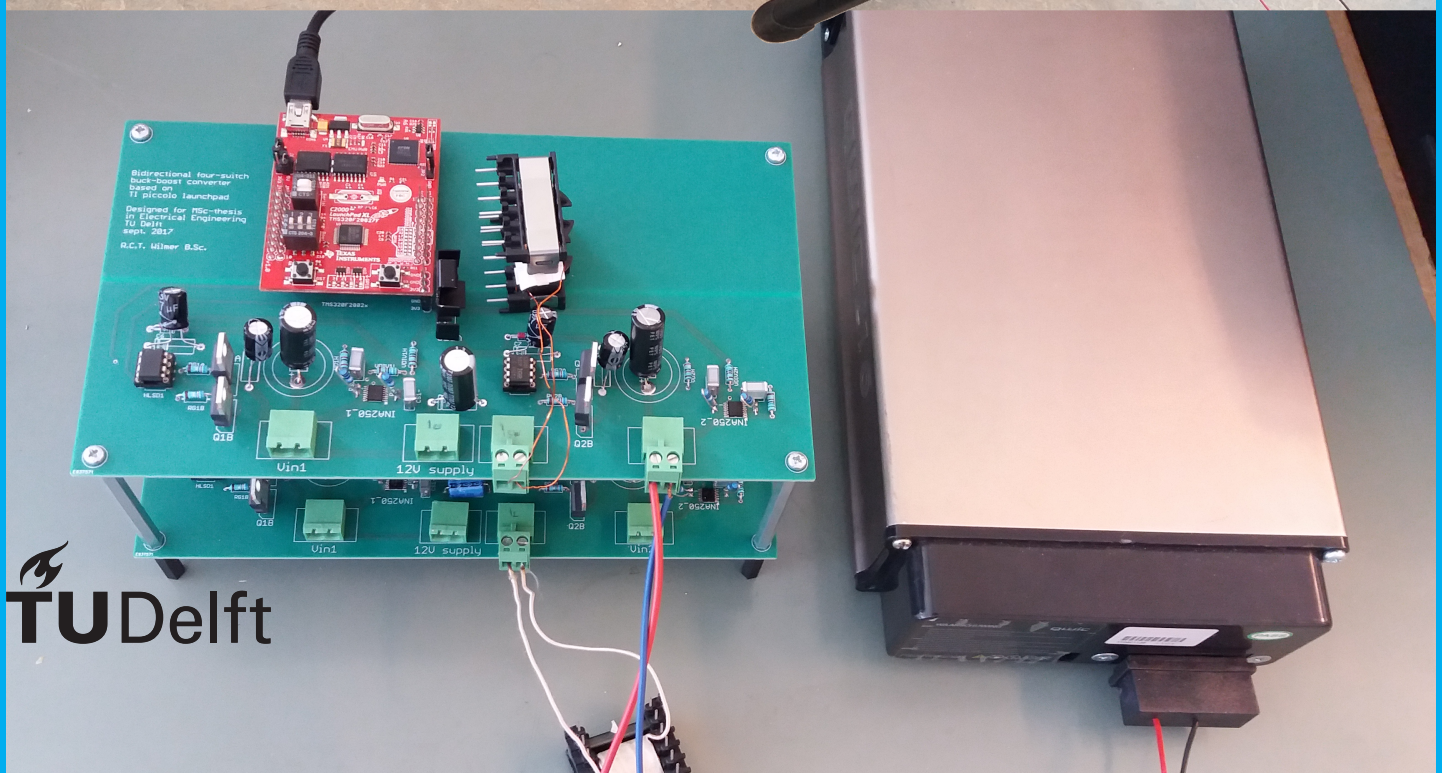

TU Delft

Control of a three-port converter for human power

by

R.C.T. Wilmer BSc

to obtain the degree of Master of Science
at the Delft University of Technology,
to be defended publicly on Wednesday October 11, 2017 at 9:00 AM.

Student number:	4137426	
Project duration:	May 1, 2016 – August 31, 2017	
Thesis committee:	Prof. dr. ir. P. Bauer,	TU Delft, supervisor
	Dr. Zian Qin,	TU Delft
	Dr. O. Isabella,	TU Delft

An electronic version of this thesis is available at `http://repository.tudelft.nl/`.

TU Delft

Preface

This thesis is the result of research conducted on a three-port converter for human power and completes the study for the degree of Master of Science in Electrical Engineering. These past years at the TU Delft, starting as a freshman and growing via a Bachelor Electrical Engineering into the study of Master of Science, can be summarized as a great journey.

In these years I have learned, experienced, contributed and gained an incredible amount. I would like to thank my parents, TU Delft staff and students, with a special word of thanks to Pavel, the PhD student who supported me throughout the thesis process, and was a valueable guide in the research. Also I would like to thank the study assocation, which has provided coffee and opportunities for relaxation whenever needed.

I focused my track within the education of Electrical Power Engineering on electrical machines and power converters. Wishing for not a purely theoretical MSc project, the realisation of a Human Power generator was proposed. I hope this thesis will serve others in the practical construction of a small-scale power converter based on a switched mode DC-DC converter topology, shining a light on all considerations necessary.

As the ancient greeks already mentioned: ἡ φύσις οὐδὲν ποιεῖ ἅλματα: nature doesn't jump. This effect is exploited to transfer power in switched mode power supplies, where energy is stored in inductor currents and capacitor voltages.

R.C.T. Wilmer BSc
Delft, September 2017

Contents

Nomenclature

DC	Direct current, not changing polarity
AC	Alternating current, a waveform which changes polarity regularly
V	Voltage
i	Current
R	Resistance, the ratio between voltage and current
P	Power, the product of voltage and current
E	Energy
t	Time
f	Frequency
ω	Angular frequency, $\omega = 2\pi f$
C	Capacitance, the ratio between charge and voltage
L	Inductance, the ratio between flux and current
SMPS	Switched-mode power supply
PWM	Pulse-width modulation, a control technique based on rectangular pulses
D	Duty cycle
S	Switching signal
Q	Denotes a semiconductor device; usually a transistor.
Q	Can be used for the quantity of charge, measured in coulombs
ρ	Resistivity of material. $\rho = R\frac{A}{l}$
σ	Conductivity, $\sigma = \frac{1}{\rho}$
l	Length
A	Area or cross-section
V	Volume
N	Number, amount. In inductor theory: amount of turns of wire
r	Radius
d	Diameter
δ	Skin depth. In a conducting wire: the depth at which the current density in a wire has dropped to $\frac{1}{e} \approx 37\%$ of the current density on the outer surface.
μ_0	Magnetic permeability of vacuum, a constant defined as $\mu_0 = 4\pi \cdot 10^{-7}$
μ_r	Relative permeability of a material
ϕ	Magnetic flux

B Magnetic flux density, $B = \phi / A$

H Magnetic field strength, $B = \mu_0 \mu_r H$

$\mathscr{F}$ Magnetomotive force, $\mathscr{F} = Ni$

$\mathscr{R}$ Reluctance, $\mathscr{R} = \frac{\mathscr{F}}{\phi}$

χ Magnetic susceptibility of a material

PMSM Permanent magnet synchronous machine, a type of AC machine

BLDC Brushless DC, an electrically commutated DC machine type

PMDC Permanent magnet DC, a mechanically commutated DC machine type

Totempole: A transistor pair, connected drain to source (in case of MOSFETs). Usually connected between Supply positive and Supply negative, to switch either rail to the midpoint.

Combined PWM mode: A switching mode for a four-switch converter where one of the two totempoles is always on, in order to reduce $\frac{\mathrm{d}i}{\mathrm{d}t}$ and smoothen out energy transfer trough the device

Reduced Combined PWM mode: In Combined PWM mode of a four-switch converter, to avoid $0.9 < D < 1.0$, both duty cycles are divided by 0.9 to ensure $D < 0.9$, but the ratio of D1 to D2 is equal.

1 Introduction

This introductory chapter will entail the structure of this thesis and the project it is based on. The thesis will consist of this introductory chapter followed by a literature review. Chapters 3 and 4 focus on electrical design and control design. The design is simulated and verified through construction of a prototype, which is described in chapters 6 and 5, respectively. This thesis concludes with conclusions on this work and recommendations for future work. In the appendices, additional pictures and graphs are presented on results of prototype testing, as well as the PCB layout.

1.1. Background

The incentive this thesis is based on aims to increase people's health by challenging them to work-out on a regular basis. This asks for a platform which aids in the stimulation of working out. Every day, a lot of people are diagnosed with diabetes or obesity. Roughly 61700 per year, or 1200 per week, in the Netherlands alone [5]. This can be reduced by a healthy lifestyle, incorporating for example regular exercise. To make working out even more attractive, the output energy of the workout is converted to electricity and stored for later use. This concept of clean energy should appeal to the customer. Not only does this promote human health, it also spreads awareness about the amounts of energy we use every day.

The envisioned platform consists of a bike-stand with generator and a user interface, which keeps track of the energy going in and out of the system and instructs the user how to use the system properly. It controls the power flow in the generator, the battery and to the system output by controlling the voltages on the peripherals.

In 2013, G. Villias wrote his MSc thesis [25] on human energy, which also included human and mechanical factors. In an extra project in 2016, Ryan Prakoso made a demonstrator model, converting human energy from a provided e-bike to electricity stored in a battery, based on a boost converter [21].

This thesis will extend existing work with energy storage by designing, building and controlling a robust three-port converter.

Currently available in literature and products is already quite some knowledge on human power. Studies have researched the possible power levels that could be harvested from several human motions [20]. One study already investigated a smart grid for a sustainable gym [16].

Cardiologist Gheroge Pop from Radboud UMC Nijmegen has actively promoted this project, also having submitted our abstract for publication.

From the cooperation with cardiologist Gheorge Pop from the Radboud UMC Nijmegen, it became clear that way too many people are diagnosed with diabetes or obesity[5]. A solution is to stimulate people to exercise more, that's where this project provides a suitable platform, which aims for people to become healthier, make them more aware of the energy used everyday, as well as generate some electricity. This can help offset the used energy in gyms, for example.

Some papers only propose a theoretical solution.This project brings both theory and a demonstration of health and electrical factors: human health through cycling, human power because of generation, and research into a three-port converter that connects rectification to battery and grid-connection.

1.2. Research questions/objectives

The main contribution of this project is to investigate behaviour of DC-DC converters in a real-world scenario. This includes accurate models of the system and converter, and waveforms measured on the prototype. The designed converter will connect energy production to storage and to a proper use of the electrical energy. The main design factor of the prototype is to be cheap, as the device could be adapted for sale on the market. It has to reliably and efficiently extract power from a human that is cycling on a stationary bicycle. The energy is stored in a battery and can be deliverid to a DC grid (or AC grid by means of a grid-tied inverter).

Research questions aid in structuring the research and drawing conclusions. The research questions will be answered throughout the thesis. The objectives are:

- Propose a three-port converter for efficient conversion of energy on a stationary e-bike with battery connected to a 48 V DC bus
- Design a controller which ensures the efficient conversion and constant (w.r.t. angle of rotation) torque on the rear wheel, so the exercise will resemble general work-out, or riding a bike on the road.
- Validate the design through simulations and construction of a user prototype

2

Literature and theory

2.1. System overview

The designed system converts the generated electricity into an energy storage system (a battery, and a grid to remove energy from the system), while delivering information about the activity (time and set intensity of the exercise, pedalled energy, power levels, state-of-charge of a battery, etc.) to the user. At the input of the system, the user will place his/her own bicycle in a bicycle-stand and start exercising. The system can be divided into five parts as seen in figure 2.1.

- Mechanical interaction; The bike with adjustable settings which depend on the user (i.e. saddle height), the mechanical power flow from pedals to the rear wheel; and the bike stand.
- Electromechanical conversion from the mechanical domain to the electrical domain: the generator.
- Electrical conversion; the rectification and conversion to storage and load.
- Processing unit; which handles all information and decision-making based on measured voltages (and currents) and power set-points. It generates switching signals to the converters. It provides the user with feedback.
- The storage and load, which will store energy or remove the energy from the system: for example a connection to a 48 V DC-bus powering small home appliances.

This research focuses on evaluation of the overall performance and performance of the electrical subsystems. To sketch a more graphic view of the system, figure 2.2 is provided.

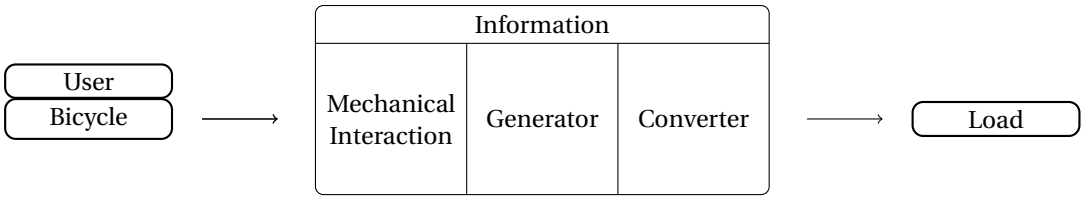

Figure 2.1: An abstract view of the system

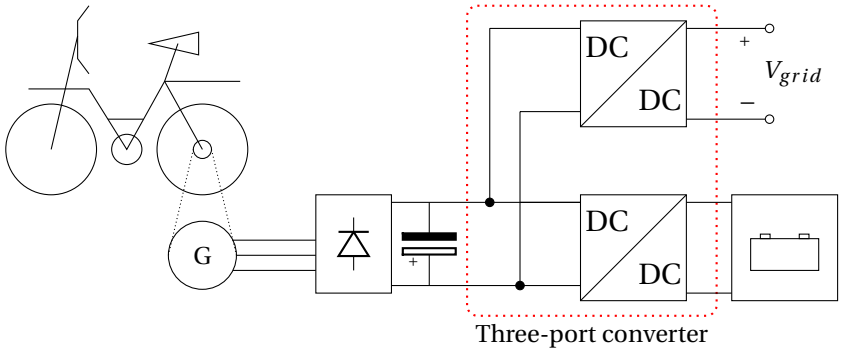

Figure 2.2: A sketch of the circuit

The electrical heart of the system can be classified as a three-port converter as it has three points where power enters or leaves the system: a dedicated input (the bike-generator system), storage (a battery) and output to the grid.

In this chapter the background on three-port converters is presented. First the input of the system, the human energy, is described. Thereafter a section is devoted to the peripherals (generator, battery and output). Lastly, the specifications and possible topologies of the converter itself are discussed.

2.2. Theory on human energy

To control the power flowing through the system, knowledge of how it is generated is crucial. Several studies on human power generation have been conducted in the past, of which [12] [written 1999] is notable. It lists multiple types of human power (active and passive mechanical movement, as well as more chemical energy usages such as skin potential and body heat), their possible power levels and power levels of equipment, thus sketching a road of possible solutions for future research.

The mechanical part of the system consists of the human, the stationary bicycle with its drivetrain, and the rotor of the generator. Factors that could affect the generated power output are, among others: bicycle posture (a recumbent position results in a comfortable workout. Breathing is easier and experienced fatigue is reduced), gear ratio, crank length, generator characteristics, etc. Influences of these non-electrical factors are stated in previous work, such as the MSc-thesis of G. Villias [25]. Furthermore, the user will tend to (or is stimulated to) find the best settings that make a comfortable exercise for him/her.

A human body can provide the most power at the leg muscles. From person to person, his/her physical condition varies. This influences maximum power available, maximum reserve of energy and the optimal cycling rate. For each individual there exists a comfortable and most efficient pedalling speed. At this optimal speed, the human legs deliver the greatest power. This varies greatly from person to person, but lies at around 50 rpm to 70 rpm, and produces up to 200 W.

These rates are ideal as the oxygen uptake is minimal (known in literature as the energetically optimal rate or EOR). Another measure for a good pedalling frequency is the rate at which minimum neuromuscular fatigue occurs, which is called biomechanical optimal rate (BOR). At long exercises under 200 W, these rates coincide around 50 rpm to 70 rpm.

2.2.1. Two-parameter energy model

To predict the available energy and power pre human, models have been developed. Studies have categorized the power available for work-out by a two-parameter model, modellinmecg the energy reserve and the power level which can be sustained indefinitely [18]. One of these parameters is called Critical Power, defined as: “that power setting representing the upper limit for prolonged work; a power that could in theory be maintained indefinitely”. A. Jansen [11] showed that critical power can be related with comfortable or sustainable force exertion.

The other parameter is the Anaerobic Work Capacity, it is an energy reserve which is available on demand. It can be used at whichever rate required. Exhaustion of the human occurs when this supply is fully depleted. The optimal work-out power, where exhaustion occurs exactly when the workout time has expired, is then this indefinitely sustainable power level plus the energy reserve divided by the desired work-out time: $P = P_{\text{indefinite}} + \frac{E_{\text{anaerobic}}}{t_{\text{exercise}}}$.

Energy in consumer products

Product	Intake [kJ]	Duration [h]
4-inch american-style pancake (thick)	85	0.157
Mars chocolate bar	260	0.481
Cookie with apple-based filling	320	0.593
Potato crisps, natural taste	902	1.670
Total energy associated with one cup of coffee (including brewing, harvesting, etc.)	1940	3.593

Table 2.1: Energy levels of consumer products and equivalent exercise duration times(at 150 W).

These power and energy levels vary from person to person, but can be determined from at least two tests. The users starts fresh and exercises until he/she is exhausted at a set power. From the different times to exhaustion from each power level, the Anaerobic Work Capacity and the Critical Power can be determined. From this model, a desired work-out time will predict an optimal work-out power level, at which the user exhausts exactly after the desired work-out time and maximal energy can be "extracted".

Human power levels
To compare pedalled power with the calorific intake of foods, or energy used to make coffee, table 2.1 is presented. Off course a part of the energy we humans consume is used to maintain our body and its functionalities. Roughly speaking, a small snack can be burned in half an hour. To provide the complete energy associated with making one cup of coffee, 3.5 whorth of exercise present a net zero footprint on the earth.

2.2.2. Mechanical conversion

From the legs, the feet push down on the pedals to generate a torque on the crank. This crank is connected via chain and gears to the rear-axis. The teeth ratio of the gears determine the speed ratio (and its inverse, torque ratio) between crank and rear wheel. A small amount of power is lost in friction, but chain systems are found to be 98% efficient [2].

Most bicycles provide different gears to select during a bike ride, so the user can match the speed of the rear wheel to a comfortable peddling rate of the cranks.Because the human pushes downwards on pedals rotating, the resulting torque will be a somewhat jerky motion, resulting in a minimum and maximum torque dependent on the angle of the cranks with respect to the vertical. This makes the generator less efficient than if it would be supplied with a torque which is constant over all rotational positions. This is illustrated in figure 2.3. If efficiency is of extreme importance, elliptical gears could be used to smoothen out the generator torque, providing a torque ratio which is the inverse of the "jerk-ratio". The shape of the gears depends on the level of jerk compared to the average torque. To use elliptical gears well, the user has to cycle with exactly the correct ratio of jerk: human can cycle exeptionally jerky (up-down) or try to smoothen this out (as circular as possible).

2.3. Theory on peripherals

The converter connects electrically to the energy input from the stationary e-bike, storage to battery, and output: the connection to a power grid. These parts, which determine the design constraints of the converter, are discussed in detail in the next sections.

2.3.1. Generator

For use as a generator, different types of machines with different output voltage (called back-EMF) characteristics exist. Because of differences in construction of different generator types, several output voltage (called back-EMF) shapes exist.

Electrical machines (motors) can classified according to the type of rotor, and the voltage shape used to drive the machine. The rotor can be either made from wound wire (and excited in order to create a flux), or constructed from permanent magnets (which do not need excitation). The stator can be excited with AC or DC. A DC voltages needs to be commutated twice per rotation of a pole-pair: either with carbon brushes or electrically. Electrical commutation alternates a constant DC to produce a block-signal. Carbon brushes introduce losses and wear out over time.

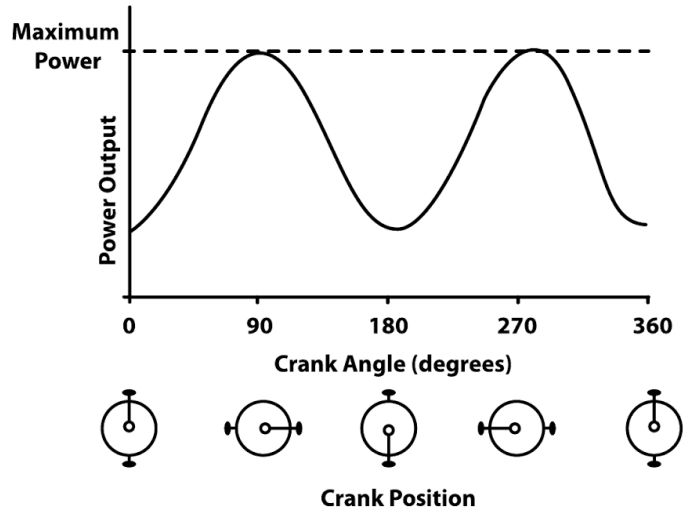

Figure 2.3: An impression of pedalled torque [4]

AC generators with wound rotor are either asynchronous (induction machines) or synchronous. Induction machines are found to be less efficient. A synchronous machine would need another source of excitation. AC generators with rotor magnets generate either a sinusoidal or trapezoidal back-EMF, which depends on the stator construction: if the wires are distributed in a sinusoidal or trapezoidal shape. The trapezoidal type is called brushless DC (BLDC), machines with sinusoidal back-EMF are called permanent magnet synchronous machines (PMSM).

		Rotor field	
		Wound	Magnet
Waveform	DC	DC-machine	Permanent magnet DC (PMDC)
	AC	induction or synchronous	Permanent magnet synchronous machine (PMSM) or Brushless DC (BLDC)

Table 2.2: Machine types, compared to method of excitation and generator waveforms.

The book of P.C. Sen [23] explains the different between wound-rotor and permanent magnet machines, as well as induction or synchronous AC machines: “Unlike the salient-pole field structure of the conventional DC motor, permanent magnet motors have a relatively smooth stator structure. Because of the absence of the field windings, copper loss is absent and this increases efficiency. No space is required for field windings; consequently, these motors are smaller than corresponding wound-pole motor and, in some cases, cheaper as well.”,. PMDC motors have a definite cost advantage in the smaller size range.

As a generator, induction machines have poorer performance characteristics compared to other types. A synchronous machine needs two excitation sources, but it has good control. Often these were big machines. However, at constant frequency these machines could reach a high efficiency, and the machine is capable of power-factor control.

The big advantage of permanent magnet synchronous machines (PMSM) is their compact size and robustness. It is therefore widely used in the industry, especially as electronics to control the motor improve. It will however mean that the back-EMF has a sinusoidal shape. To be coupled to a DC-generator, this output voltage has to be rectified and filtered with a (large enough) capacitor.

AC generators can generate either one-phase or three-phase voltages. Three-phase voltages provide a more constant power (by nature) and its rectified voltage shape has a smaller ripple. At same power and rated voltage, a three-phase system will carry significantly lower currents.

Modelling of an electrical machine

To predict the electrical behaviour of an electrical machine, a simulation model consisting of all equations that describe the electical behaviour was implemented and tested in different scenarios. Not everything can - or has to be - modelled. Some aspects of the real-world behaviour are not of main interest, for example

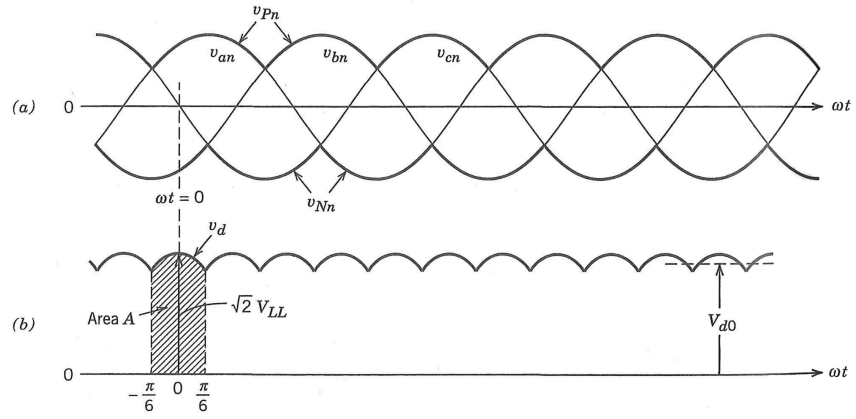

Figure 2.4: Three-phase rectifier input and output voltages [17]. Figure (a) shows the three-phase phase-to-neutral voltages, with output voltages highlighted, for the electrical period of 2 rotations or 4π. Figure (b) shows the rectified voltage, which has period $\frac{\pi}{3}$ of the input voltage (or 6 pulses per input period), and amplitude of $\sqrt{2}$ times the input line-to-line voltage.

mechanical oscillations. Simulating extra detail leads to extra simulation time. On the other hand, some behaviour can not be captured with a simple set of equations.

A model which can be used to describe most permanent magnet machines consists of a speed-dependant AC voltage source, a resistance which models the losses in the machine, and an inductance to account for storing energy in the magnetic fields. As the induced voltage is proportional to the derivative of the flux, a linear dependancy on both amplitude and frequency is established. An example is shown in figure 2.5. The ratio of speed to output voltage amplitude is called the voltage constant. As mechanical power and electrical power are equal (in approximation), the ratio of torque to output current is the inverse of this voltage ratio.

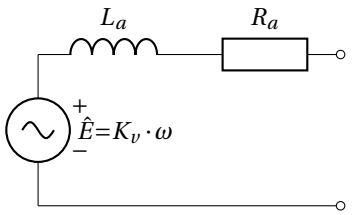

Figure 2.5: An equivalent single-phase model of an electrical machine

$$v = \hat{E}=K_v \cdot \omega \tag{2.1}$$

2.3.2. Battery

Using storage of generated energy should be done in newly designed electrical systems, as local generation makes storage desirable. It accumulates energy for later use, which can be used for peak shaving; at the moments where a household consumes the most energy of the day (so when people wake up, or when they come home from work and start cooking), the stresses put on the grid can be lowered by using locally generated electrical energy. By generating and storing electricity locally at cheaper rates, such a system becomes economically feasible.

Modelling of the battery

To ensure safe use of a battery, its status should be predicted. Supplying the battery with a too high or too low voltage might infer excessive currents, leading to unsafe operation. The battery is also modelled in the controller. Different models are available. Which to use depends on the trade-off between complexity and accuracy. If the current stresses put on the battery are not too high (a portion of the capacitiy rate) and slowly varying (with respect to the internal time constants), a simple battery model can be used. But when high

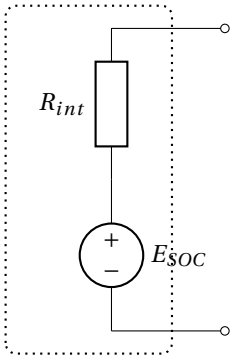

(a) Equivalent simple model of a battery

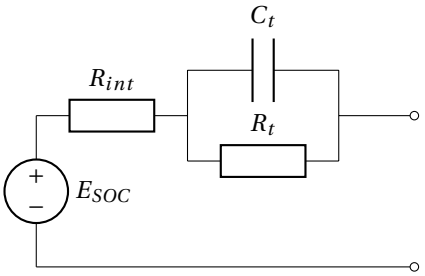

(b) Equivalent model of a battery, with RC-branch to model transients

Figure 2.6: Comparison between battery models

currents or highly varying currents apply, a more detailed modelling of the battery will have to be studied. So per application a different most suitable model exists.

A battery has an internal voltage (called open-circuit voltage OCV or back-emf E) which appears at the terminals when open-circuited. This voltage varies nonlinearly with the internal state of charge (SOC). The terminal voltage has a small dependance on state of charge in the working range of 20-80% charge. Near full charge or discharge, the voltage rises or falls sharply. The resistance through the battery is modelled as an ohmic resistor, of which the value can be derived empricially or by datasheet.

The battery is (dis-)charged by supplying a voltage slightly higher or lower than this internal voltage, leading to a voltage drop over the internal impedance and a current $i = \frac{V_t - E}{R_{int}}$ to flow. These (dis-)charging currents cause losses and thus heat. If the currents exceed safe levels, temperature rise could lead to irrevertible damage, leakage or even explosion of the battery cell.

Models can be classified in mathematical models and equivalent circuit models [10]. Mathematical models fit variables to data by least root mean square error estimation. It uses a voltage expression dependant on back-emf, resistive voltage drop and an estimated SOC-dependant variable; $V_t = E_o + R \cdot i + f(SOC)$. Equivalent circuit models model an electrical circuit, using a combination of resistances, capacitors and diodes to describe the current-voltage relationship at the input. Equivalent circuit models provide a better accuracy and are able to dynamically predict the behaviour.

The simplest model consists of the open-circuit voltage OCV and an internal resistance R_{int}. Transient behaviour can be modeled by adding a parallel RC-combination. Additional equivalent models are suggested and tested in [8]. The RC-model can be expanded with a variable which is called un-available charge by the authors[1], but this has some purpose only in situations where the current changes dynamically. An even more detailed model can be found in a mathematical model called the adaptive extended kalman filter (AEKF) [26], which uses kalman filtering to estimate.

In this project a roughly constant power will be drained during exercise, so the battery current won't be too dynamic, with a rather constant power going into it. To keep the complexity of the models manageable, a simple electrical model with one RC-network to model transients will be implemented, as depicted in figure 2.6b.

2.3.3. Load

The generated energy will be transported to an electrical grid eventually. The power can be redirected into a DC-bus of for example 48 V, a low-voltage solution comparable to technologies which are investigated by TU Delft. The converter can be connected to AC-grids, requiring a grid-tied inverter (GTI), which have been exhaustively researched by industry and are not within the scope of this thesis. Using a DC input voltage, the grid-tied inverter injects power from the system into the grid at synchronous AC voltage.The amount of energy that will flow into the grid should be the generated input power minus battery power, minus losses, which is controlled by the system controller.

2.4. Theory on converters

The generated AC voltage at the output of the generator, with variable frequency and amplitude, could be converted directly to the 50 Hz AC-grid voltage and frequency. This would however require large components, which are only tuned to one input voltage and frequency. By rectifying the input voltage to DC and using a high switching frequency (i.e. 100 kHz), a desired output voltage can be synthesized. And the dominant switching frequencies, that require filtering, are orders of magnitude higher so filter components can be made much smaller. On top of that, control of these switching converters is more flexible due to faster dynamics.

Some voltage regulators use linear conversion. Input and output current are equal, but the voltage is stepped down through a voltage divider network with feedback, acting as a variable resistor. The excess energy is dissipated as heat. This is a simple and cheap solution, but is inefficient, creates significant temperature rise, and is not capable of stepping up voltage.

As input voltage and output voltage are not equal, an indirect way of transferring energy should be accomplished. Connecting input and output voltage through an inductor will achieve current flow, with the voltage difference charging the inductor current: $V_L = L\frac{\mathrm{d}i}{\mathrm{d}t}$ or $\mathrm{d}i = \frac{V}{L}\mathrm{d}t$. To keep the current within bounds, the inductor has to be alternatively charged and discharged. The ratio of charging to discharging times should be ratio of voltages over the inductor, to keep Δi average zero.

On the other hand, switched-mode power supplies (SMPS) are capable of producing output voltages both higher and lower compared to input voltage, and are more efficient, as well as capable of handling larger powers than linear voltage regulators. Energy storing devices such as inductors and capacitors are switched with high frequency to shape desired voltages and currents. The fundamental equations governing capacitor and inductor voltages and currents are stated in equations (2.2) and (2.3)

$$i_C = C\frac{\mathrm{d}V}{\mathrm{d}t} \tag{2.2}$$

$$V_L = L\frac{\mathrm{d}i}{\mathrm{d}t} \tag{2.3}$$

2.4.1. Topologies

Several topologies of switched b DC-DC converters are known. These are classified into isolated and non-isolated topologies. Non-isolated topologies are buck, boost, buck-boost, SEPIC, zeta and Ćuk. Isolated topologies such as forward, flyback, push-pull, half-bridge of full-bridge offer galvanic isolation between input and output. Transformer output windings can be added or changed (during design) to provide different output voltages. Non-isolated topologies however add more components for the same functionality, so in this research they are not investigated. The complete system (bicycle, battery, converter) can be referenced to the ground of the output grid.

The three most fundamental converters discussed in literature are the buck, boost and buck-boost converter topologies. The output voltage of these topologies range from 0 to V_{in}, V_{in} to ∞, or 0 to ∞, respectively. Given input voltages that can be both higher and lower than output voltage, only the buck-boost converter would be suited of these three choices. On top of that, more advanced topologies exist, which are - among others - the SEPIC, zeta (or inverted SEPIC) and Ćuk converter. Both are also capable of stepping up or down the voltage. These have a voltage ratio similar to the buck-boost converter, but solve some issues of the buck-boost converter. The most notable differences lie in the continuity in input and/or output current; the buck-boost converter has switches in the main current path, thus requiring relatively large filter capacitors to keep input and output current continuous. The Ćuk converter has two inductors in the current path, and only switches to ground. This results in smooth currents. The connection of inductors and capacitors is however rather complex to control.

Adding possibilities make the converter more expensive and complex, whereas this research aims for a cheap converter. Therefore a buck-boost is used. Any other topologies than the ones mentioned above use more switches, therefore these are not considered.

Inverting buck-boost converter

The most basic buck-boost topology, which only compromised of one inductor and two switching elemtents and is called the inverting topology, is drawn in figure 2.7. The inductor current is charged with V_{in} and discharged with $-V_{\text{out}}$. In steady-state pulse width modulation (PWM) of the switch with a duty cycle D denoting the fraction of on-time of the first switch compared to the total period, the output voltage is given

by (2.4) - derived from the volt-second balance across the inductor.

$$V_{\text{out}} = -\frac{D}{1-D} V_{\text{in}} \tag{2.4}$$

The output has negative polarity with respect to input voltage. The switch is in the current path, which means the midpoint (from which the driving voltage for the transistor is referenced) floats at $+V_{\text{in}}$ or $-V_{\text{out}}$. The chip driving the switch has to be able to withstand the negative voltage. The input and output current are discontinuous, as the switches (or diode) are in the current path of both the input and the output.

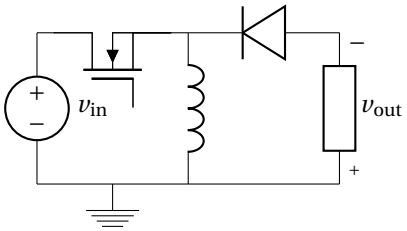

Figure 2.7: An inverting buck-boost converter

Four-switch buck-boost converter

An alternative to connecting the inductor with one terminal to ground and the other to $\pm V_{\text{in}}$ and V_{out}, is to switch one terminal to 0 or V_{in}, and the other to 0 or V_{out}. The same voltages over the inductor can be realised, but output voltage is positive with respect to input voltage. This buck-boost topology is realised with four switching elements, resulting in the same relationship between output and input voltage ($V_{\text{out}} = \frac{D}{1-D} V_{\text{in}}$) as the inverting buck-boost converter topology. Four of the semiconductors can be replaced by diodes, but making the 2 diodes actively controlled allows for reversing the current direction through the converter. Another advantage of MOSFETs is a lower voltage drop during conduction($I \cdot R_{DS,on}$) than a diode (0.8 V), with $R_{DS,on}$ typically <0.1 Ω. More on bidirectionality is explained in section 2.4.2.

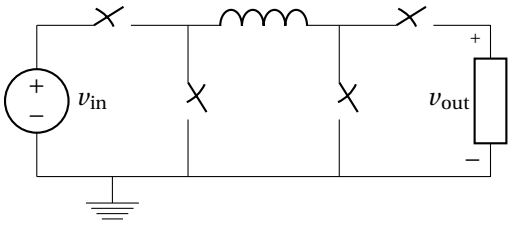

Figure 2.8: A four-switch buck-boost converter

SEPIC and zeta converter

One of the “advanced” DC-DC converter topologies include the SEPIC and zeta converter (also called the inverted SEPIC). In figure 2.9 it is shown that these converters share a common “prototype”. It resembles a boost-converter followed by a buck-boost converter. If the prototype is read from left to right, the prototype resembles a zeta converter. If read from right to left, the prototype resembles a SEPIC converter. The difference between the two is the direction of the power flow. The SEPIC has continuous input current and reduced input voltage ripple, the zeta has continuous output current and reduced output voltage ripple. This is an advantage of the zeta converter, as more often the load is sensitive to output ripple, than the input is sensitive to current ripple. In this case, the converter is explicitly called a zeta converter. For example, in some power supplies the output needs to feed a device with a fairly constant voltage, fed by a wide range of input voltages.

If the current will be unidirectional, one semiconductor can be a transistor, the other a diode. This implies that the SEPIC configuration has the switch connected with the source terminal to ground, whereas the zeta configuration has a highside switch (floating) in the current path. If the current is bidirectional however, both semiconductors need to be actively driven, so two transistors are needed. This means that the topology could be named both SEPIC or zeta, depending on the main current direction. More on bidirectionality is explained in section 2.4.2.

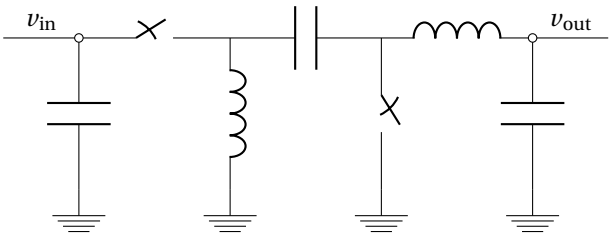

(a) A prototype converter for SEPIC or zeta

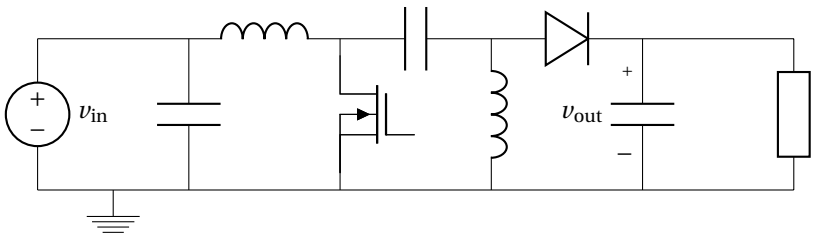

(b) A SEPIC converter

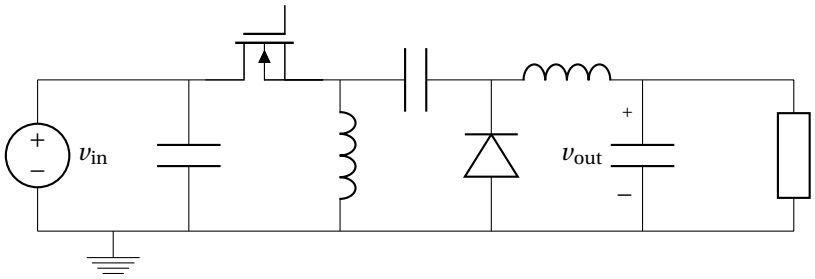

(c) A zeta converter

Figure 2.9: Three converters

A drawback of the SEPIC technology is that it takes a fast switching diode (with low voltage drop for efficiency reasons) to avoid voltage spikes over the inductor. Fast conventional diodes or Schottky diodes may be used.

Another drawback of these topologies with more components in the main current path, is that resistances in the capacitors and inductor influence ripple and efficiency, possible to a large extent. A capacitor type with a low ESR (equivalent series resistance) should be used, as the capacitors handle large currents which frequently change direction.

Microchip however states that this topology is difficult to control due to multiple dynamic components interacting (the capacitors and inductors make a fourth-order transfer function from input to output) [22]. Another drawback is that "the main switching node goes below ground". This refers to the high-side switch which is in the current path. In a practical application, not every chip can withstand negative voltages there.

TI, commenting on the control of the dynamic system, states in its application note [6]:"The zeta converter is a fourth-order converter with multiple real and complex poles and zeroes. Unlike the sepic converter, the zeta converter does not have a right-half-plane zero and can be more easily compensated to achieve a wider loop bandwidth and better load-transient results with smaller output-capacitance values". (...) "The drawbacks are the requirements for a higher input-voltage ripple, a much larger flying capacitor, and a buck controller (...) capable of driving a high-side pmos".

The practical implementation of this converter promises to have some complications, among others the 4^{th} order nature of the topology, due to multiple energy storing devices (capacitors and inductors), influencing eachother. As a bidirectional converter, the advantages of SEPIC over zeta (or vice versa) will cancel out due to the converter carrying current in both directions: if one current direction has advantages, at reversal of power flow the converter will lack these advantages.

Ćuk converter

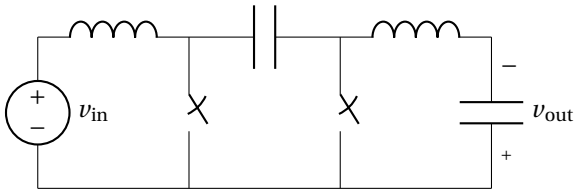

Figure 2.10: A Cuk-converter

The Ćuk converter (the new topology first proposed by S. Ćuk and R.D. Middlebrook in [3], is drawn in figure 2.10) has both continuous input current and continuous output current, as no switching elements are in the current path. The switching elements pull either side of the capacitor to ground, controlling the voltage over the inductors indirectly. This results in a system which is also complex to control, but both input and output current are continuous. Another drawback is the inverted output voltage of the Ćuk converter, which the controller needs to be able to handle.

2.4.2. Bidirectionality

A battery is both charged and discharged so the converters connected to storage operate in two current directions. To allow for bidirectional current, all semiconductors are controlled semiconductors such as MOSFETs. The voltages lie in the same quadrant for the two modes of operation.

DC-DC converters as usually presented in literature are designed for unidirectional current. If a switching element carries current opposite to the voltage blocking direction, it can be represented by a diode as shown in figure 2.11. Because a bidirectional converter has switching elements which need to carry current in both directions, these can't be diodes; in that case, all switching elements will be implemented with MOSFETs. If the internal body diode of chosen power MOSFETs turns out significantly slow, it can be enhanced with an antiparrallel Schottky-diode.

2.4.3. Summary

The advantages and disadvantages of the mentionend converter types are shown in table 2.3.

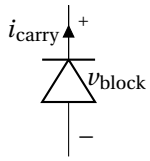

Figure 2.11: A semiconductor which carries current opposite to blocking direction.

Topology	**Input current**	**Output current**	**Complexity**	V_{out}
Inverting	DIScontinuous	DIScontinuous	Order 2	Inverting
Four-switch	DIScontinuous∗	DIScontinuous∗	Order 2	
SEPIC	continuous	DIScontinuous	Order 4	
zeta	DIScontinuous	continuous	Order 4	
Ćuk	continuous	continuous	Order 4	Inverting

Table 2.3: Overview of currents in selected topologies. Discontinuous currents need a relatively large filter capacitor.

2.5. Magnetics

This section focuses on the theory behind magnetic field. First, the relationship between B and H is treated, especially in inductors used for switched mode power supplies. Losses in the core and in the copper of such an inductor are considered. Lastly, the theory of magnetic circuits is presented. This is a modeling technique which uses the equations of magnetomotive force $\mathscr{F}$, flux ψ, and reluctance $\mathscr{R}$, to predict the real-world behaviour in magnetic components.

Inductance is the property of an inductor at which rate a current will generate a magnetic flux. Even a single wire has some inductive properties, but often this has little effect. In order to increase self-inductance of a wire, it can be wound in a coil to locally enhance the magnetomotive force, as more wires contribute to the flux at one point, and more wires are affected by this flux.

The inductor's main property of self-inductance L can be defined as the ratio of flux to the current that created it. In the induction equation $V = \frac{\mathrm{d}\phi}{\mathrm{d}t}$ it links current and voltage trough $V = L\frac{\mathrm{d}i}{\mathrm{d}t}$.

In a coil, $L = \frac{N\phi}{i}$ or:

$$Li = N \cdot BA \tag{2.5}$$

With current i, number of turns N and B the flux density and A the cross-sectional area the fluxlines pass through.

To reduce the number of turns in an inductor and to concentrate the magnetic field, the wire can be wound around a core made of ferromagnetic material, which provides a low reluctance path for the magnetic flux. The core material enhances B with a factor μ_r, this is a property of the ferromagnetic material. But the energy stored in magnetic field in the core also reduces by a factor μ_r, which is significant as for most ferromagnetic material the relative permeability $\mu_r \gg 1$ (typically 500-2000). An air gap can be introduced to store more energy, which also stabilises the total reluctance of the inductor: the core material properties fluctuate due to temperature and frequency effects.

$$E = \frac{1}{\mu_r}\frac{1}{2}B^2 Al \tag{2.6}$$

2.5.1. Ferromagnetic materials

Ferromagnetic materials are classified either as "soft" (which are easily magnetised, but don't remain magnetised after the external field is removed) or "hard", which do remain magnetised.

If an external magnetic field H is applied, small subdomains in the material align their magnetic moments in line with the external H field, creating more flux. The magnetisation is related to the total flux density as $B = \mu_0(H + M)$. Often, the magnetisation field is proportional (via the magnetic susceptibility χ) to the external magnetic field strength, thus it can be written: $B = \mu_0(1 + \chi)H = \mu_0\mu_r H$, with μ_r the relative permeability, which acounts for the amount of magnetisation of the material.

$$B = \mu_0\mu_r H \tag{2.7}$$

At higher magnetic field strengths, the material becomes (fully) magnetised, and an increase in H won't increase B as much as at to lower magnetic field strengths. The factor μ_r thus becomes smaller. This effect is referred to as saturation. In datasheet, often the relation of μ_r to H is specified.

The magnetic material exhibits magnetic coercivity, which means that if magnetized, the domains keep their orientation of magnetisation. At a magnetic field strength $H = 0$, some magnetisation remains, and thus $B = \pm B_r$, dependant on the previous sign and magnitude of H. To get the B-field to zero, an amount of $H = \mp H_c$, called the coercive force is applied. A typical BH-curve is shown in figure 2.12. The area enclosed by the two graphs is related to the work needed to magnetise the material. It is dependent on the maximum applied H: For higher values, the loop widens. Each cycle, this work represented by this area is dissipated as heat. Losses in the core due to hysteresis thus increase with frequency.

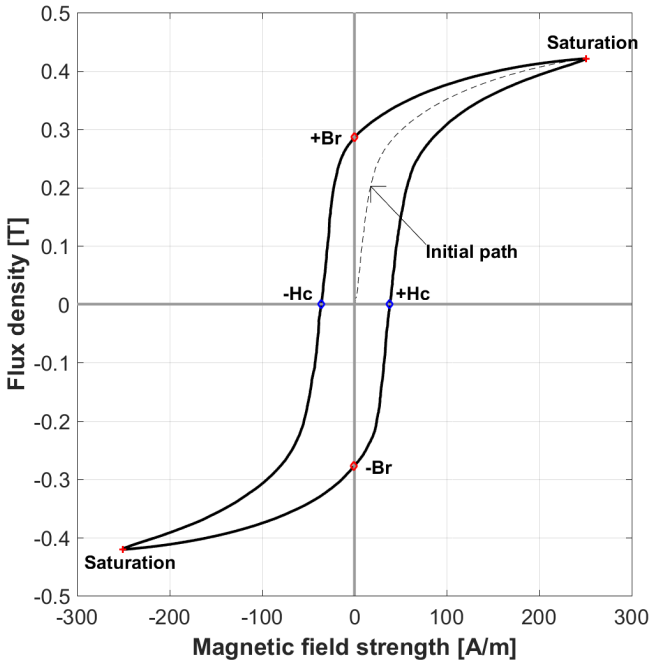

Figure 2.12: A typical hysteresis curve for ferromagnetic material.

At saturation, an increase in current through the inductor will result in a (realitvely) smaller increase in flux density; the apparent inductance will decrease. Therefore saturation should be avoided.

2.5.2. Magnetic circuits

Just as the electric circuit describes the behaviour of voltage and current, a magnetic circuit can be used to solve the equations governing the behaviour of magnetomotive force $\mathcal{F} = N \cdot i$, flux density and reluctance $\mathcal{R} = \frac{\mathcal{F}}{\phi}$.

A coil with N turns, carrying a current i, around magnetic core with relative permeability μ_r and gap with length l_g can be described by a circuit with a magnetomotive force and two reluctances, one describing a uniform core, the other representing a uniform airgap, as is illustrated in figure 2.13. A reluctance describes the ratio between current-turns and the total flux. It doesn't dissipate energy, but stores a magnetic energy. The magnetic flux likes to take the path of least reluctance. The product of Ni makes a flux over the series combination of core reluctance and gap reluctance. The air gap reluctance is higher than the core reluctance. The flux lines try to contract in on themselves, and puch eachother away (fringe) to try to minimise the energy stored in the magnetic field. This fringing results in a reduced reluctance (thus higher inductance) and can be accounted for by increasing the air gap area with a factor F_{fr} in the calculations. For prototyping, this factor will be neglected (considered ≈ 1) and in the iterative design of the inductor, its effect will be dealt with indirectly.

It has also been approximated with formulae in literature. Some examples are stated: In equation (2.8a) William T. McLyman [15] approximates the flux fringing by the ratio of gap length to one side of the cross-

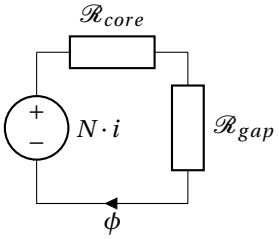

Figure 2.13: The model of the magnetic circuit in a single inductor with a core and air gap. The equivalent reluctance $\mathscr{R} = \frac{l_e}{\mu_0 \mu_e A_e}$

section and the natural logarithm of the window length to half the air gap length. In equation (2.8b) Marian Kazimierczuk [13] approximates the flux fringing by extending the core dimensions (width and height off the cross-section) by the gap length, times gap length, and comparing this to the cross-section $a \cdot b$. In equation (2.8c) Hurley and Wölfle [9] approximate the flux fringing by extending the core dimensions (width and height off the cross-section) by the gap length and dividing by the original area. However, all such equations are only approximate, and usually work only under the assumption that the length of the air gap is much smaller than any of the dimensions of the core.

$$F = 1 + \frac{l_{gap}}{\sqrt{A_e}} \cdot ln\left(\frac{2 \cdot l_{window}}{l_{gap}}\right) \tag{2.8a}$$

$$F = 1 + \frac{l_{gap}\left(a + b + 2 \cdot l_{gap}\right)}{a \cdot b} \tag{2.8b}$$

$$F = \frac{(a + l_{gap}) \cdot (b + l_{gap})}{a \cdot b} \tag{2.8c}$$

To summarise, the reluctance can be calculated as in equation (2.9).

$$\mathscr{R} = \frac{l_{gap}}{\mu_0 A_e \cdot F_{fr}} + \frac{l_e}{\mu_0 \mu_r A_e} = \frac{1}{\mu_0 A_e}\left(\frac{l_{gap}}{F_{fr}} + \frac{l_e}{\mu_r}\right) \tag{2.9}$$

Linking the inductance with the magnetic circuit theory, the following equation is derived, which describes flux, flux density, inductance and reluctance, by means of number of turns and current trough the inductor.

$$N\phi = Li = \frac{N^2 i}{\mathscr{R}} = BA \tag{2.10}$$

2.5.3. Current distribution in the inductor conductors

Due to AC current producing and being affected by magnetic fields, the current distibution in inductor wires will not be uniform. This leads to a reduced equivalant area, thus an increase in equivalent resistance and losses in the copper of the inductor. These are also due to eddy currents: as any time-varying current radiates a time-varying magnetic field, this time-varying magnetic field will induce so-called eddy currents in nearby conductive material, including the wire itself. This results in a non-uniform current distribution over in the conducting material.

If the currents affects the same conductor it runs through, this effect is called skin effect: the current tends to flow (at higher frequencies) only at the edges or “skin” of the wire. The *skin depth* δ is defined as the distance from the surface at which the local current amplitude is decreased by a factor e from the surface. The AC resistance will increase significantly from this frequency on. The skin depth can be calculated from equation 2.11. In design, the wire radius should be smaller than this skin depth, for the wire size to be regarded as effective.

$$\delta = \frac{1}{\sqrt{\mu_0 \mu_r \sigma \pi f}} \tag{2.11}$$

For copper this formula can be approximated as, $\delta = \frac{65}{\sqrt{f}}$. In adjacent wires, the current will tend to flow only in the innermost layers of the copper that carry the same current. So after winding, the AC-resistance will even increase over the AC-resistance of a single wire. Therfore, a design should be made for a certain frequency, to be able to incorporate the increased losses. To measure this AC-resitance, RLC-meters often have the capability to measure resistance as well, at varying frequencies.

Any conductivity in the core material will also result in induced eddy currents, which result in additional losses and are dissipated as heat.

2.5.4. Litze wire

One solution to suppress high-frequency effects is found in litze wire. An illustrated example of how Litze is constructed is shown in figure 2.14.

Litze wire is a cable made from several insulated strands, each with radius smaller than the skin depth, in order to suppress skin effects. The wire is specified as 140×0.071: 140 strands of 0.071 mm diameter each. This way, a high-frequency current can be carried in a conductor with low resistance. To ensure all strands are connected to a terminal, the ends can be dipped in heated tin, as to melt away the individual insulation and ensure a tin connection across the conductor.

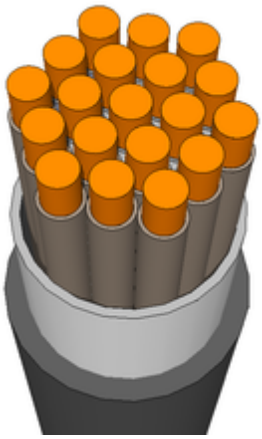

Figure 2.14: An illustrated example of a Litze wire consisting of 19 strands.

3

Electrical design

In this chapter the electrical design is presented: from expected circumstances, scenarios, interaction, inputs and desired outputs the topology, components, ratings and values which are calculated to give the best overall performance. Best performance depends on the demanded specifications; which factors or parts of a trade-off is stated as most important.

The following sections will each explain the design possibilities of the system parts: user, mechanical interaction, electromechanical converter, electrical converter, storage and energy output. Specifications on hardware, input and output voltages, currents and powers will be discussed.

The user is the human that pedals and generates power. It is an input to the system so no design choices can be made, but a proper estimation of the behaviour and power levels is vital for the design. It is expected that he/she will be an average (dutch) human (not regarding athletes). This means the user exercises for 0.5 h to 1.0 h, with power levels at 100 W for comfortable exercise, or peaking to 200 W. The user will adjust the bicycle to his/her needs (body lengths etc), and is instructed to do so. The desired duration and power setting for the exercise is set. The user can be aided with estimating time and intensity, by keeping a profile of his/her exercises and fitting the two-parameter model as discussed in section 2.2.1. During the exercise, the user is provided with feedback on how much energy and power is (and has been) generated, and battery status; the rate at which it is being charged or discharged, and the state of charge.

3.1. Mechanical interaction

The mechanical interaction encloses the system from the human pedalling on a stationary bicycle to the electromechanical converter. Both seating and exercising must be comfortable for the user.

The mechanical energy must be converted from the crankshaft to the generator efficiently and at correct speed ratio, matching the preferred pedalling rate of a human during long exercises (50 rpm to 70 rpm) to the rated speed of the generator, which can be designed for.

Varying aspects of a bicycle - held upright on a bike stand - can be categorised according to ease of changing them:

1. Aspects that can be changed during work-out are the gearing (on bicycles with multiple gears). User input (torque and speed) will vary during work-out.

2. Aspects that can be changed in-between workouts or users are bicycle settings such as saddle height, handlebar position, etc. Small maintenance such as lubricating the chain and gears can also be done before or after a work-out.

3. Aspects that vary per bike or are hard to change are crank length, crankshaft gear shape (round vs. elliptical), individual gears (i.e. replacing a sprocket by a sprocket which has a different number of teeth in order to change possible gearing ratios), riding position (upright bicycles or recumbant bicycles) or wheel diameter.

The bike should be adjustable to fit multiple users in a healthy way to avoid injuries. Ideally, the user can use his/her own private bicycle, which is of course set to the user preferences.

Most bicycles offer different gearings to choose from. From an electrical standpoint, a faster rotating rear wheel is preferred: Higher rotational speeds lead to higher induces voltages in the generator, as these are proportional to the change in magnetic flux captured by the coils. A higher voltage reduces losses in the electrical domain at a same transmitted power, as $P = V \cdot i$ and ohmic losses are proportional to $P = i^2 R$. In AC generators, a faster rotational speed also implies a higher electrical frequency, resulting in a more stable rectified DC-link voltage: a shorter time between pulses reduces voltage ripple as $\mathrm{d}V = \frac{i}{C}\mathrm{d}t$. As humans prefer to pedal at a rate of 50 rpm to 70 rpm, a high gear ratio is thus preferred. From gearboxes available for bicycles designed for use on road, highest or second to highest gear ratio is advised. A too high rear wheel speed will result in mechanical problems such as losses, so extremes don't have to be sought after.

Changing gears can be done by a derailleur or a hub-mounted gear box with internal gears. Different hub and derailleur gearboxes from different brands were compared in the journal Human Power. The following (numbered) conlusions arose [2]:

1. "Efficiency generally increases with the load—for all transmissions"

2. "Hub gears are generally about 2% lower in efficiency than derailleur-type gears. But there are exceptions. "

4. "With modern transmissions, where multiple gears are available, there is often a difference of 1% to 3% in efficiency between adjacent gears. An average 2% difference in efficiency is thus easily possible if the wrong gears are chosen."

5. "The tests show that some gears are inefficient."

This indicates that in practice, the type of gearing doesn't matter too much as efficiency can vary per gear. For the design, a few percent can be gained by using derailleur gears. Lubrication of the transmission is also of importance to reduce mechanical losses.

3.2. Electromechanical converter

The generator has to be able to convert the generated mechanical energy from the user into electricity efficiently. If possible it has to be rather cheap. The generator must be able to handle the maximum power levels which are to be extracted.

As stated in chapter 2.3.1, a DC-generator is less efficient and its carbon brushes have to be maintaned. An AC machine with permanent magnets is most suited because of the compact size, smooth behaviour and reliability. Looking at rectification, three-phase systems have a smaller current ripple compared to single-phase systems, which is beneficial to efficiency. The chosen type is therefore a three-phase permanent magnet synchronous machine, which has a sinusoidal back-emf.

Main differences between the types of AC machine (BLDC, PMSM and induction generators) are stated in [24]. A PMSM has higher efficiency, better torque-size ratio and wider speed range than induction machines. PMSM and BLDC have a similar construction, the only difference lies in the windings which are wound with sinusoidal distribution instead of trapezoidal. PMSM are more efficient and have a smaller torque ripple (and noise) than BLDCs.

The book of Mohan [17] argues in favor of three-phase converters (over single-phase AC), as the current drawn from a rectifier has less ripple and less distortion. "...that the current in a practical single-phase rectifier contains significantly more distortion compared to a three-phase rectifier. This results in a much poorer power factor in a single-phase rectifier compared to a three-phase rectifier.(...) The ripple current, which flows through the filter capacitor, dictates the capacitance and the current-handling capability required of the filter capacitor. Therefore, in some applications, the filter capacitance required may be much smaller."

As for the power levels, the human is expected to pedal up to 200 W. For safety and durability, a rating of 250 W is a good measure. Compared on the mechanical level to a single-phase motor, a three-phase motor has no cogging effect so pedaling is smooth and no vibrations are created. Humans cycle most effective around 50 rpm to 70 rpm. Through a high gear ratio of 3.14, the rated speed of the machine should be approximately 160 rpm to 220 rpm.

3.3. Electrical converter

The electrical converter has to handle the three-port power flow between input (generator), storage and output. The electrical converter can therefore be seen as the heart of the system.

Several variables or aspects can be chosen or tuned. The biggest choice is that of the converter topology, on which the control and sizing of components depend.

From expected inputs of the system, a topology and its components can be designed according to rated voltages. Along with topology, an appropriate control method and frequency are selected. After sizing the components, a detailed design of the inductors is treated.

3.3.1. Topology

For battery-operation, an isolated converter topology is not needed. This provides galvanic isolation (input and output are electrically disconnected, but may be coupled by magnetics through a transformer, for example) but would add components; thus increasing size, costs, complexity and losses. Only non-isolated topologies are considered. Non-isolating topologies that produce output voltages both higher and lower than input voltage are buck-boost, SEPIC (and inverted SEPIC) and Ćuk topology. The buck-boost topology is relatively easy to make and control. It has however a discontinuous input- and output current, which need larger input and output capacitors for filtering. Whereas the buck-boost converter topology is rather simple to control, the SEPIC and Ćuk converter are two more complex DC-DC converters, due to four energy storing elements, which can give rise to non-linear behaviour. A SEPIC (or zeta) converter has continuous input (or output) current. The Ćuk converter topology has a continuous input and output current: smaller filtering capacitors are needed. Apart from the switching semiconductors, it has however three components in the main current path; this is more than the buck-boost converter, which has only one inductor carrying the main current.

A simulation showed that with real components, losses in components and semiconductors were significantly higher with the same control: A PWM-controller with fixed duty cycle of $D = \frac{V_o}{V_i+V_o}$. Because of improved efficiency and cost, a (robust) buck-boost converter is preferred over a Ćuk converter.

3.4. Rated voltages

In order to size the converter, input and output voltages and powers are to be known. This is to ensure proper working of the converter. If the operating conditions exceed designed safe operating conditions, among others the converter can't be controlled, or the currents may exceed safe operating levels.

The input voltages were measured from a provided experimental set-up from previous work. The DC voltage after rectification of the generator voltage was measured to be minimum 16 V at a minimum input cycling rate of 45 rpm and middle gear (at ratio 2.2). At top gear (of ratio 3.14) and a high cycling rate, up to 70 V was achieved. As the battery is fused at a maximum of 4 A the absolute maximum current for the battery converter was set at 4 A.

Under a threshold value of fore example 10 W, the system is shut off. The grid converter should take the excess power (desired input power minus the battery power). It can be inactive ($P = 0$) or take full battery power plus human power (400 W total).

The design constrained values are summarized in table 3.1

3.4.1. Frequency selection

To size the components, the expected PWM frequencies need to be decided. Deciding on this frequency is a trade-off between efficiency, dynamics and component sizing. The higher the frequency, the higher some equivalent series resistances become (for example copper losses due to eddy currents in wires with radius

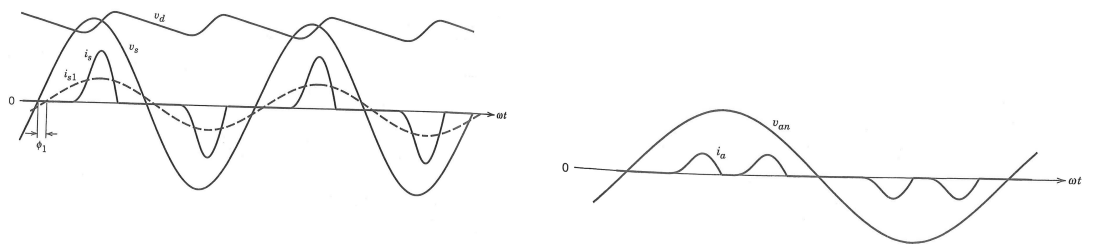

(a) Single-phase rectifier voltage and current

(b) Voltage and current of one phase of a three-phase rectifier

Figure 3.1: Comparison between single-phase and three-phase rectifier currents with inductive source [17]

	Min	Nom	Max	Unit
V_{in}	16	30	70	[V]
P_{in}	10	100	250	[W]
I_{in}	0.625	3.3	4	[A]
V_{batt}	30	36	40	[V]
P_{batt}	±10	±100	±144	[W]
I_{batt}	±0.3	±2.7	±4	[A]
V_{grid}		48		[V]
P_{grid}	0	100	400	[W]
I_{grid}	0	2	4(8)	[A]

Table 3.1: Ranges (minimum, nominal and maximum) of input, storage and grid values for the converters

greater than skin depth), leading to increased conducting losses. Switching losses increase with frequency as well, due to a linear increase in switching actions per second.

A higher frequency means less energy will have to be stored in between switching actions, and thus the energy storing devices needn't be as big. It also allows for the system to react quicker to transients. It also allows for smaller components to be selected, both in value (µF)and packaging.

Actual frequency on which the converter will run is a trade-off between size and controllability. A too high frequency will require fast control, which the controller should be able to provide. Losses (and thus temperature) in the inductor will also rise with higher frequencies. As an absolute lower bound, 25 kHz is selected as any acoustic noise produced by for example magnetostriction of the core will be audible to the human ear.

To follow common practices, the design stated frequency-dependent components (such as minimum inductance value L and filter capacitors C) are also stated as a value-frequency product; for example $L \cdot f$ and $C \cdot f$. Next, the input rectifier stage is designed.

At a slow expected input of 45 rpm pedalling rate at the max gear ratio of 3.14, the rectified output voltage has an electrical frequency f_e of 621.7 Hz and a period between the rectified pulses of 1.6 ms. At the maximum load of 4 A, the minimum required rectifier capacitance which allows for a voltage drop not greater than 2 V is: $C = i_{\max} \frac{\mathrm{d}t}{\mathrm{d}v} = 3.2\,\text{mF}$.

3.4.2. Buck-Boost design

The buck-boost topology was presented in chapter 2.4.1. Each switch needs to be able to block the maximum input voltage of 70 V. The set maximum current to flow through any of the devices in this topology is 4 A.

The inductance value is sized from the constraint that at minimum average current and maximum voltage difference over the inductor, the current won't drop to zero. Maximum voltage drop over the inductor happens when the converter supplies 70 V into the 40 V battery. The minimum average current was set at 0.25 A. The peak inductor current is then twice the average input current, divided by main duty cycle.

$$L = \frac{V_i \cdot DT_s}{2\frac{I_{in}}{D}} = 0.5\frac{V_i V_o^2}{I_{in}(V_o + V_i)^2}\frac{1}{f} \tag{3.1}$$

Results are summarised in table 3.2. It can be seen that the worst-case inductance is required for the highest input voltage, of 70 V. At 100 kHz an inductance of at least 185 iHs required to keep a current flowing in the converter.

L in µH	V_{in}	
f (kHz)	10 V	70 V
50	256	370
100	128	185
200	64	93
500	25.6	37

Table 3.2: Minimum inductance values of L (in µH) for different frequencies, at output voltage $V_o = 40\,\text{V}$ and $I_{av} = 0.25\,\text{A}$

3.4.3. Output capacitor

The output voltage should be maintained rather constant for control- and output stability, as well as filtering the output current. In order to regulate a voltage at the output, the inductor (which has a current-character) should discharge into the capacitor, which has a voltage-character. Even at maximum load current of 4 A, the voltage should be regulated within 1% of the output voltage of 40 V, which equals 0.4 V. The maximum dt is the longest on-time of the input switch, as stated in equation 3.2

$$\mathrm{d}t = \frac{C\mathrm{d}v}{i} = D \cdot T_s = \frac{V_o}{V_o + V_i}\frac{1}{f_s} \tag{3.2}$$

Results are shown in table 3.3. It can be seen that the worst-case capacitance is required for the lowest input voltage, of 10 V. At 100 kHz a capacitance of at least 80 µF is required to keep the output voltage within bounds.

C_{out} in µF	V_{in}	
f (kHz)	10 V	70 V
50	160	72.73
100	80	36.36
200	40	18.18
500	16	7.27

Table 3.3: Minimum capacitance values for different frequencies, at output voltage V_o = 40 V and I_{max} = 4 A

Name	Value	
C_{rect}	3.2	mF
$\Delta V_{\text{rect,max}}$	2	V
V_{block}	70	V
I_{conduct}	4	A
$\Delta V_{\text{out,max}}$	0.4	V
D_{min}	0.2	–
D_{max}	0.8	–
f	50 - 500	kHz
$L \cdot f$	18.512	HHz
$C_{\text{out}} \cdot f$	8.00	FHz
L(100 kHz)	185	µH
C_{out}(100 kHz)	80	µF
C_{grid}(100 kHz)	83	µF

Table 3.4: Summary of designed values for bidirectional buck-boost converter to battery

3.4.4. To grid

The second buck-boost converter is designed to convert from the rectifying input capacitor to a 48 V DC-grid. The worst duty cycle now happens when a voltage is converted from 10 V to 50 V (to be able to inject power into the 48 V grid), as D = 0.833: $C = i\frac{\mathrm{d}t}{\mathrm{d}v}$ =83 µF

3.5. Losses

To compare losses in three converters, a quick simulation was performed in MATLAB Simulink. Results are summarised in table 3.6. Settings of the possible parameters are shown in 3.5. A buck-boost, run in both a Complementary ($D_2 = 1 - D_1$) and a Combined ($D_1 = 1 or D_2 = 1$) mode, is compared to a Ćuk converter. A Ćuk converter has two transistors compared to the 4 of the buck-boost converter, but has two inductors and a capacitor in the main current path. The Ćuk converter is found to be less efficient. The reduced losses in MOSFET transistor come from the fact that the Ćuk converter only has 2 transistors.

Name	Value	Unit
Buck-boost inductor value	2	mH
Ćuk L1 inductor value	1	mH
Ćuk L2 inductor value	1	mH
Inductors series resistance	0.2	Ω
MOSFET on resistance	0.1	Ω
MOSFET body-diode resistance	0.01	Ω
MOSFET body-diode forward voltage	0.3	V
MOSFET snubber resistance	100	kΩ
MOSFET: no on inductance		
MOSFET: no (= ∞) snubber capacitance		

Table 3.5: Simulation values to compare buck-boost(PWM), buck-boost(Combined PWM) and Ćuk converter

	Buck-boost topology	Ćuk converter
Total losses	1.335	2.696
In transistors	0.834	1.04
In the inductor(s)	0.501	1.656
Total energy out	22.89	22.825
Energy efficiency	94.17%	88.2 %

Table 3.6: Energy losses (in J): Results of comparison of buck-boost topology and Ćuk converter, for a simulation during s

3.6. Magnetic design

The design of an inductor entails multiple variables and multiple factors to account for. Often the design is a iterative process: after an initial design, specifications and requirements are checked. After (a series of) small adjustments, a final design is obtained. The prototyping of an inductor can differ from what has been calculated due to approximations and assumptions which are neccessary to make calculation, but that introduce errors in predictions, that differ from the real world.

Inductor designs vary, depending on what design requirements are stated. Some design focus on reliability (for example in aerospace engineering) or extreme efficiency. The design of this thesis will aim at a cheap inductor, as the envisioned product should reach as wide of an audience as possible and make it for insurance companies as interesting as possible to refund the product based on exercise (thus improving human health and lowering insurance expenses due to treating people with diabetes or obese people).

3.6.1. Design process

This next section identifies the parameters that influence the design and which part imposes these. Several constraints are imposed or calculated, coming from:

- The electrical circuit
  - Minimum inductance value L of 190 µH
  - Maximum current that will flow through the inductor i_{peak} of 4 A
- The geometry of the core:
  - Winding window: The space enclosed by core material, where the current carrying wires are supposed to run. Both height and width are specified.
  - The effective cross-sectional area of the core A_e
  - The effective length l_e, the path through the core where fluxlines will run. These two parameters, along with the relative permeability of the material, define the reluctance of the core.
- The core material
  - Relative permeability μ_r depends on the material type chosen.
  - Maximum flux density B_{max}, at which the material doesn't saturate

  - Core losses, due to hysteretic losses: The area in a BH-curve of a material represents the losses per cycle, as explained in section 2.5: each half-cycle, an amount of energy is used to align the magnetic subdomains in the ferromagnetic material.

- The chosen wire type
  - The diameter of the wire restricts the number of turns that fit inside the winding window.
  - The lost power in the wire is proportional to the equivalent resistance (at the chosen design frequency). Due to skin effects, the current distribution in a conductor will become less uniform with higher frequencies, thus increasing resistance. The wire radius should be chosen smaller than the skin depth. More on skin depth is explained in 2.5.3. Choosing Litze wire can mitigate high-frequency effects.

- External wishes
  - The product should be cheap, thus using a confined amount of material: the smallest core which has a big enough winding window.

One of the variables which vary per design is for example the maximum core flux density. It has to be chosen low enough to avoid saturation, but the exact figure is often a result of the iterative process. If reliability is one of the requirements, the flux density will be chosen relatively lower to narrow the BH-curve (thus reducing losses), increasing the durability of the inductor. In core and wire type, a range of possibilities exist. To start, an educated guess is made. After the design, it is checked if a parameter should be adjusted. For inductor design, two main formulae are used, stated in (3.3) and (3.4). With l_{gap} the air gap length and F_{fr} a ratio to account for fringing factor, the relative increase in cross-section of the flux as the fluxlines bulge out in the air gap.

$$\phi = \frac{Li}{N} = \frac{Ni}{\mathscr{R}} = BA \tag{3.3}$$

$$\mathscr{R} = \frac{l_{gap}}{\mu_0 A_e \cdot F_{fr}} + \frac{l_e}{\mu_0 \mu_r A_e} = \frac{1}{\mu_0 A_e}\left(\frac{l_{gap}}{F_{fr}} + \frac{l_e}{\mu_r}\right) \tag{3.4}$$

The self-inductance L is the total flux generated by a certain current, or $L = \frac{N\phi}{i}$. With $\phi = B \cdot A_e$, the equation which can be used for design is shown in equation 3.5. The maximum current i_{peak} is given by electrical characteristics. The maximum allowable flux density B is chosen by hand, but depends on the saturation level in the core material. A_e is the effective core cross-section (accounting for fringing and other non-idealities), often specified in the datasheet of a chosen core type.

$$N = \frac{L \cdot i_{peak}}{B \cdot A_e} \tag{3.5}$$

This results in the minimum number of turns that will ensure $B < B_{max}$ at peak current. Adding more turns will decrease the peak density and reduce core losses. In rounding this number to an integer, it should be rounded up to ensure the minimum number of turns is reached.

The effective inductance is then expressed as in equation 3.6, with subscript $_e$ denoting effective values. ϕ is solved from the magnetic circuit equation: $Ni = \phi\mathscr{R}$

$$L = \frac{N\left(Ni\mathscr{R}^{-1}\right)}{i} = \frac{N^2}{\mathscr{R}} \tag{3.6}$$

If the inductor has no ferromagnetic material in the core (such as air), a B_{max} cannot really be defined. But to reach the minimum inductance value, a big number of turns are needed, as $\mu_r = 1$. With a core fully made of magnetic material, the inductance is often too high for the desired electrical behaviour, as $\mu_e >> 1$, at 500-2000. A solution is to incorporate a small gap of low-permeability material (such as air) in the core. Some manufacturers make gapped cores, or core material with voids with non-magnetic material insid, thus distributing the air gap. This minimum gap can be calculated by using theory on magnetic circuits.

As the magnetomotive force applies over these reluctances in series, $Ni = B \cdot A \cdot \left(\mathscr{R}_{core} + \mathscr{R}_{gap}\right)$, the gap length is calculated by assuming the reluctance of the gap to dominate in the total reluctance. Then the air gap reluctance becomes $\mathscr{R} = \frac{l_g}{\mu_0 \cdot A} = \frac{Ni}{B \cdot A}$. To solve for the air gap, equation (3.7) is used.

$$l_{gap} = \frac{Ni\mu_0}{B} \tag{3.7}$$

3.7. Choosing Wire

When choosing wire, a lowest impedance is preferred: choosing bigger wire will result in a reduced resistance. Due to skin effect, at high frequencies the effective area decreases - and ohmic losses increase - by a factor

$$\frac{A_{skin}}{A_{round}} = \frac{2\delta r - \delta^2}{r^2} = 2\left(\frac{\delta}{r}\right) - \left(\frac{\delta}{r}\right)^2 \tag{3.8}$$

A chosen core geometry also dictates a winding window: the maxmimum area that can be occupied by wires. On top of that, fully packing the winding window will reduce thermal conductivity, leader to higher temperatures in core and copper, leading to less-than-ideal circumstances, such as reduced inductance, lower saturation levels, termal runaway, thermal failure. Not using more than ≈ 80% of the winding window is advised. The minimum number of turns that have to fit here were calculated in equation (3.5).

3.8. Losses

During energy transfer through the inductor, some energy is lost due to copper losses in the winding of the inductor. This is characterised in the equivalent series resistance. Not only in the wires but also in the core itself losses are present:

- Hysteresis losses. Due to hysteresis, work is required to magnetise the material, which is proportional to the area of BH-loop. The losses can be estimated as $P_{hyst} = k_h \cdot f^x \cdot B^y \cdot V_e$, with V_e the effective Volume of the core. The constant k_h and the exponents x and y are depedant on the core material, and should be provided by the manufacturer.
- Eddy current losses: when a magnetic flux passes a conductive layer, it induces a current in that layer. The losses can be estimated as $P_{ec} = k_e \cdot f^2 \cdot B^2$.
- Residual losses, due to (among other) irregularities in the core material. These comprise a small portion of the total losses but are hard to calculate.

So per material, the characteristics need to be provided by a datasheet! Saturation must be avoided for proper functioning of the circuit (the slope of $\frac{\mathrm{d}B}{\mathrm{d}H}$ changes - and thus the inductance value L), but also to prevent thermal runaway. To decrease influences of the temperature etc. on the total reluctance, the air-gap reluctance should be bigger than the core-reluctance

The design for an inductor which is made of the smallest core halves (ETD29) and 3C90 material at different frequencies is stated in table 3.7. Design for 2x smallest core:

f (kHz)	L (µH)	N	air gap (mm)	Winding usage (%)	$\hat{B}$ (mT)	R_{dc} (mΩ)	R_{ac} (mΩ)	$\frac{R_{ac}}{R_{dc}}$
50	370.24	43	0.474	61.48	456	19.10	46.34	2.427
100	185.12	22	0.243	40.98	456	8.68	28.66	3.304
200	92.56	11	0.121	20.49	456	4.13	18.78	4.553
500	37.024	5	0.055	20.49	456	1.88	13.20	7.038

Table 3.7: Design for 2x smallest core

3.9. Driving of the semiconductors

For use in switched mode power supplies, MOSFETs and diodes are used. MOSFETs are charge-controlled transistors, with the conductivity of the channel between drain and source dependent on the applied charge (voltage) on the gate. MOSFETs can be produced in two types: N-type MOSFET (which have electrons as charge carriers) or P-type MOSFET (which have holes as charge carriers). The electron mobility is roughly 2.3 times higher than hole mobility, which results in the main differences between N-type and P-type (gate-capacitance, channel resistance, input noise, cost, size, trans-conductance, thermal rating, etc.), advantageous to N-type MOSFETs.

The potential difference between gate and source terminals modulates the main conducting channel (between drain and source). If this gate-source voltage exceeds a certain threshold level, the device will start to conduct, the MOSFET is called “on”. The gate-driving voltage needs to thus be referred from the source terminal. If the MOSFET has to conduct a positive voltage (higher than logic level), driving could become difficult. A designated driver has to be used to shift the drive voltage from ground to the source-terminal.

3.10. Storage

To accumulate the produced energy to be used later, it is stored in a battery. The power level of the battery (rated voltage times fused current) should accomodate all incoming energy. Excess energy can be transferred to the grid during workout, when battery is full, or after workout. To relieve the grid operator, it should be at peak energy consumption.

A typical exercise rates at 100 W to 150 W for 0.5 h to 1.0 h. This would mean one exercise can produce up to 150 Wh. To prolong battery life (reducing operating costs of the system), the battery is not operated at full range of state of charge, but only from 20% to 90%. This means the full capacity should be at least 215 Wh. Extra capacity will mean a more robust system, but also increases costs.

The rated voltage of the battery should lie in the nominal pedalling range of the bicycle (as well as close to the grid output voltage), so the DC-DC converters can operate in a efficient ‘ of operation, where the on- and off-times of the switch are not excessivly short or long compared to the control frequency.

For battery technology, a low-maintenance type is beneficial as the system is to be used at homes. [**?**] Lithium-based battery technologies don't require any maintenance and have high energy density. On top of that, Lithium-ion is advantageous as it has a low internal resistance and high cycle life.

3.11. Energy output (grid connection)

The energy output will deliver excess energy (pedalled power minus battery power) to a DC grid. For stability of the grid, a gradual power output is desired; peak loads will only affect lifetime and capability of equipment. At a power level of 100 W the battery is discharged in 1.5 fhrom 90% to 20% when the battery is not operated. If the battery is fully charged, all generated power (150 W) should flow to the grid, so exercising is not affected. The design is for a 48 V DC-bus, powering small home appliances, at up to 4 A.

4

Control design

This chapter discusses control strategies and the design of a control method, given a switched mode DC-DC converter. The control unit has the task of monitoring the system and providing the system with those inputs, that accomplish desired output - a set energy transfer - within a safe operating area. If controlled incorrectly, the system could start oscillations or other unwanted behaviour, resulting in reduced energy transfer, additional losses, or worse: damage to components with (catastrophic) failure of the system as a result. First, control schemes are introduced. After a consideration, the implementation is discussed.

4.1. Control schemes

The switching signals from the controller result in MOSFETs switching on and/or off, realising different interconnections of the system components. The capacitors and inductors store energy, which changes as a consequence of input currents and voltages. For example a current flowing into a capacitor will increase the capacitor voltage. An alternating positive and negative voltage over an inductor will charge and discharge current. This is used to control the voltages and currents in such a way, that desired operating points are reached.

Different control strategies exist, which are classified according to whether voltage or current is the controlled variable, or which parts of the switching period are controlled. Distinction can be made between constant frequency or variable frequency control techniques. Constant frequency control modes use a fixed period with repeated switching signals. Variable frequency control modes depend on measured variables.

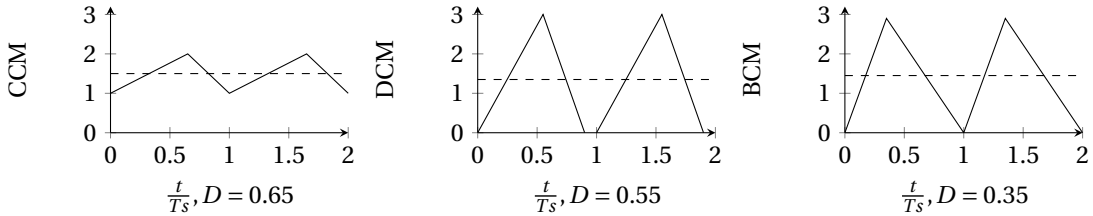

Figure 4.1: Examples of inductor current in CCM, DCM and BCM

Fixed frequency or pulse-width modulation method can be either in continuous conduction mode (CCM), where the inductor current never drops to zero, or discontinuous conduction mode (DCM), where the inductor currents reaches zero before the switch is turned on again. In boundary conduction mode (BCM), the switch is turned on exactly when the inductor current reaches zero, which results in a variable frequency of operation. These three modes of operation are demonstrated in figure 4.1

Other variable frequency control modes are **constant on-time** (waiting for the current to return to a lower boundary), **constant off-time** (waiting for the current to reach an upper boundary) and hysteresis control (in which the on-time and off-time are variable: when an upper or lower boundary is crossed, a switching action happens). These variable frequency schemes all need to measure the inductor current (direct or indirect, for example by a shunt resistor in the ground-path of switches). In constant on-time, the current is only measured during the off-time of the main switch, which flows from the C_{on}-switch through the inductor to

the output. A shunt resistor next to the C_{on}-switch is easy to measure and will provide enough information for switching. A similar case for constant on-time: only the current that flows during on-time of the switch needs to be measured, which is available next to the C_{off}-switch.

During Hysteresis mode, all parts of the inductor current need to be measured, as indicated by the word "Hysteresis" over the inductor.

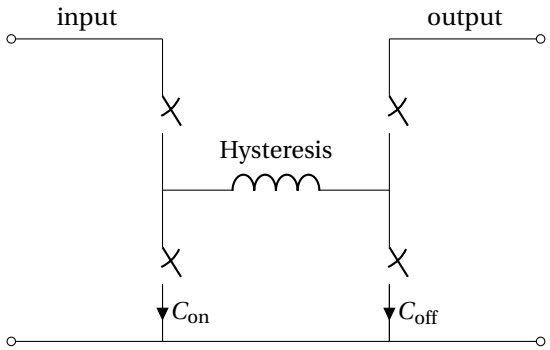

Figure 4.2: Current measurements for different control schemes

4.1.1. PWM

In a Pulse-Width Modulation (PWM) scheme, the switches are triggered on regular intervals of a fixed period. The width of the pulse (on-time) is varied, to control the output. Every period, the switch is on for a fraction - called duty-cycle D - and off for the complement of that fraction. This is demonstrated in figure 4.3.

The duty cycle influences the steady-state voltage relationships. For SMPS converters like the buck-boost, this is calculated from applying the volt-second balance over the inductor, resulting in $D \cdot V_{in} = (1-D) \cdot -V_{out}$, or (4.1).

$$D = \frac{t_{\text{on}}}{T_s} = \frac{V_{\text{out}}}{V_{\text{out}} - V_{\text{in}}} \tag{4.1}$$

PWM sets up a steady-state point for the inductor current by ratios of connection to input and output voltage, but doesn't control any internal state variables (such as capacitor voltage and inductor current). This leaves the possibility of slow or oscillatory behaviour to reach the required steady-state set-point.

PWM control is also called voltage mode control or duty-cycle control. It can be in CCM, DCM or BCM Advantage of PWM is that the DC load regulation is good. Disadvantages however are that the ability to react to dynamics is poor compared to current control: the controller gives the input and output voltages in a ratio to the inductor, charging and discharging the current. If the output voltage is too low or too high, the inductor current will be too high or too low, thus feeding into the output capacitor to raise (or lower) the voltage, until steady-state is reached: a continuous regulator is regarded as a two-pole filter system.

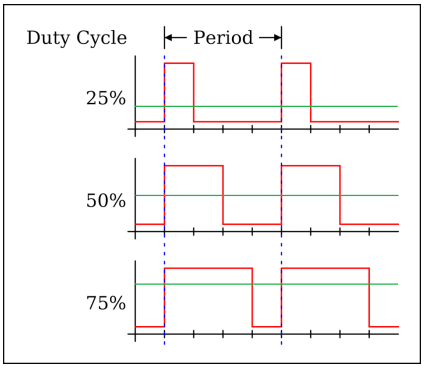

Figure 4.3: An illustrated example of Pulse width modulation and average values

4.1.2. Variable frequency control

Current control measures (a part of) the inductor current to regulate. Switching actions are not purely time-dependent, so the control modes are variable frequency control modes. Current control is actually a two-loop system: the current control is an inner (local) control around the switch to control current, the set-point of which is controlled by the (outer) voltage loop.

Three types are distinguished here: **constant on-time** (where the main switch is held on for a fixed period, then turned off until the measured current reaches a boundary), **constant off-time** (where the main switch is held off for a fixed period, then turned on until the measured current reaches a boundary), and **hystersis**

control (where the main switch is turned on at a lower boundary and turned off at an upper boundary of the measured current). Which type to use depends on which currents are easy to measure.

In hysteresis mode control, the controlled variable (inductor current) is compared to boundaries around a constant set-point. Only if a lower or upper boundary is reached, a switching action takes place, and the system is expected to reach the other boundary on itself. Hysteresis control allows for a greater dynamic range. Also less harmonics/EMI occur: the EMI is spread out over a range of frequencies. The time between switching actions depends on the amplitude between boundaries and the derivative of the controlled variable - in inductor-based switched mode DC-DC converters dependent on the voltage over the inductor and the inductance value.

If the lower boundary of hysteresis of the current is 0 A, this mode coincides with Boundary Condition Mode. If one part of the current is hard to measure, for example in a boost converter when the main switch is off, a constant-off time mode can be implemented, so no information on current is needed while it cannot be measured indirectly.

Advantages of current mode control are mainly because of control based directly on the actual inductor current, rather than on a voltage:

- Dynamics of input voltage are handled faster than with PWM.
- Simplified loop: the second order characteristic eliminated because the control loop only handles the inductor current.

  Inherent to the previous point, the controller has no loop stability problems, as the dynamics are of a first order.
- Automatic pulse-by-pulse current limiting: never will the inductor current exceed the upper boundary.
- Optimal large signal behaviour: A big step in input or load is easily controlled, as per switching action the boundaries can be set. Whereas with PWM, the current slowly increases with each duty cycle.

Disadvantages however are:

- DC open load regulation is worse: the output voltage doesn't purely rely on duty cycles but is a result of the current fed by the inductor into the capacitor.)
- Noise immunity is worse, due to a per cycle regulation.
- Higher peak/average current error and instability
- (1-D) current error in boost or buck-boost circuits, which would require slope compensation

4.2. Control choice

Due to speed, stability and that the inductor current is directly controlled (with inherent current limiting), current control is prefered above duty-cycle control. It however requires a fast and precise current measurement. To transduce the current to a voltage that can be sensed, often a shunt resistor to in the current path to ground of the switches, but the switches don't always carry the current of the inductor, so an incomplete picture is sketched. On top of that, using shunt resistors introduces voltage offsets and losses, which reduces efficiency of the converter.

Two inherent lossless current measurement methods integrate the voltage applied to the inductor, either by direct integration via an opamp, or by introducing an RC-filter with time constant equal to the LR-time constant of the used inductor. These are, among others, introduced in [7] or [19]. The filtering method was deemed most promising, as integrating with an opamp introduces additional discrete elements and cost. The filtering method is described in detail in an application note of Linfinity [14]. In short; the filter uses an RC-network to transduce the voltage into an exponentially varying voltage. The resistor acts as a current source for the capacitor, which integrates into a voltage. The time-constant of the RC-network is designed to be equal to the LR-time constant of the coil. This results in a voltage that is an (indirect) copy of the inductor current It is shown that if the L/R-time constant is greater than the switching period - and RC-time constant equal to L/R constant - the inductor current can directly be calculated from $V_{Cs} = i_L \cdot R_L$.

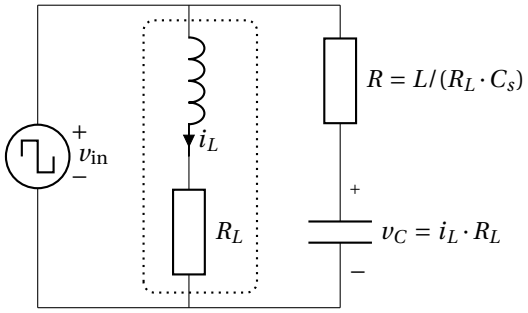

Figure 4.4: A filtering current sensing method, exploiting the inductor series resistance. As described in [7].

4.3. Control of a four-switch buck-boost converter

This section zooms in on design choices in a four-switch buck-boost converter, as shown in figure 4.5. The convention is used which labels the switches in ascending order from the input to the output as in the figure. Q1 is the switch connecting V_{in} to the positive terminal of the inductor. Q4 is the switch connecting V_{out} to the negative terminal of the inductor. Q1 and Q2 are switched complementary: If Q1 is on, Q2 is off and vice versa. States where both Q1 and Q2 are on or off are forbidden states, for it will either short-circuit the input, or open-circuit an inductor, leading to undefined voltages and induced voltage spikes. Q4 and Q3 are switched likewise.

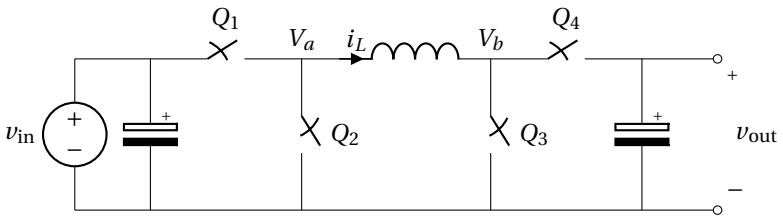

Figure 4.5: A four-switch buck-boost converter

The behaviour of a buck-boost converter is described by equations (4.2).

$$V_{\text{a}} = Q_1 \cdot V_{\text{in}} + Q_2 \cdot 0 \tag{4.2a}$$

$$V_{\text{b}} = Q_4 \cdot V_{\text{out}} + Q_3 \cdot 0 \tag{4.2b}$$

$$V_{\text{L}} = V_{\text{a}} - V_{\text{b}} = L\frac{\mathrm{d}i}{\mathrm{d}t} \tag{4.2c}$$

$$i_L = \frac{1}{L}\int V_{\text{L}}\mathrm{d}t \tag{4.2d}$$

Switching signals S1 and S2 are defined as $S_1 = Q_1 = \overline{Q_2}$ and $S_2 = Q_4 = \overline{Q_3}$:
$S_1 = 1$ if Q1 is on ($V_{\text{a}} = V_{\text{in}}$) and Q2 is off (and vice-versa).
$S_2 = 1$ if Q4 is on ($V_{\text{b}} = V_{\text{out}}$) and Q3 is off (and vice-versa).

S_1	S_2	V_{L}		V_{L}	$V_{\text{L}} \stackrel{?}{=} 0$
0	0	$0-0$	=	0	0
0	1	$0-V_{\text{out}}$	=	$-V_{\text{out}}$	<0
1	0	$V_{\text{in}}-0$	=	V_{in}	>0
1	1	$V_{\text{in}}-V_{\text{out}}$	=	$V_{\text{in}}-V_{\text{out}}$	$\neq 0$

Table 4.1: Effects of S1 and S2 on inductor voltage

$\begin{bmatrix} S_1 \\ S_2 \end{bmatrix} = \begin{bmatrix} 0 \\ 0 \end{bmatrix}$ is a useless combination; the energy stored in the inductor does not change, nor does any exchange with input or output happen. The system is in an “island-mode”. Energy transfer through the converter is not achieved.

$\begin{bmatrix} S_1 \\ S_2 \end{bmatrix} = \begin{bmatrix} 1 \\ 1 \end{bmatrix}$ is a fine combination. It results in an inductor voltage drop of $V_{\text{in}} - V_{\text{out}}$, which is of smaller absolute value than either input or output voltage, and its polarity depends on which voltage dominates. Due to the smaller absolute voltage, the inductor current rises slower, resulting in longer switching times, a smaller current ripple and reduced EMI.

4.3.1. Implementation

To enable a high and smooth energy transfer from input to output, it is prefered to have switches closed as much as possible, or as high duty cycles as possible. Allowing for input and output main switches to overlap results in a smaller $\frac{\mathrm{d}i}{\mathrm{d}t}$, and thus longer time between switching actions, as well as a lower peak value of the current; less harmonics/EMI occur, and a possible delay in switching action will cause a lower error in the current. It also ensures a (more) continuous flow of input and output current. If a transistor doesn't swtich at all (or very low frequent), significantly lower switching losses occur.

Hysteresis control

In hysteresis control, if $V_{\text{in}} > V_{\text{out}}$: if the current reaches a lower boundary, $\frac{\mathrm{d}i}{\mathrm{d}t}$ has to become > 0. Either $\begin{bmatrix} 1 \\ 1 \end{bmatrix}$ or $\begin{bmatrix} 1 \\ 0 \end{bmatrix}$ can be used, with the former option more advantageous due to aforementioned reasons. If the current reaches the upper boundary, $\begin{bmatrix} 0 \\ 1 \end{bmatrix}$ has to be used as it is the only switching combination that results in $V_{\text{L}} < 0$. Inspection shows that $S_2 = 1$, so no switching action takes place. No switching losses occur, and the output is always fed with the inductor current.

Analogous situations arise if $V_{\text{in}} < V_{\text{out}}$: $\begin{bmatrix} 1 \\ 1 \end{bmatrix}$ can be used instead if $\frac{\mathrm{d}i}{\mathrm{d}t}$ has to become < 0, resulting in $S_1 = 1$; the input main switch is held on.

PWM control

In PWM control, allowing for duty cycles of the first and second main switch to overlap, higher duty cycles can be constructed by dividing both duty cycles by the largest; one duty cycle become 1, and the ratio of the two duty cycles will still result in the voltage transfer ratio.

$$D = \frac{\frac{V_{\text{out}}}{V_{\text{in}} + V_{\text{out}}}}{\frac{V_{\text{in}}}{V_{\text{in}} + V_{\text{out}}}} = \frac{V_{\text{out}}}{V_{\text{in}}} \tag{4.3}$$

Equivalently, duty cycles can be constructed as

$$D_1 = \max\left(\frac{V_{\text{out}}}{V_{\text{in}}}, 1\right) \tag{4.4a}$$

$$D_2 = \max\left(\frac{V_{\text{in}}}{V_{\text{out}}}, 1\right) = D_1 \cdot \left(\frac{V_{\text{in}}}{V_{\text{out}}}\right) \tag{4.4b}$$

Minimal voltage drop

Allowing for both input and output switch the be on simultaneously: $\begin{bmatrix} S1 \\ S2 \end{bmatrix} = \begin{bmatrix} 1 \\ 1 \end{bmatrix}$ results in an inductor voltage difference of $V_{\text{in}} - V_{\text{out}}$. However if $V_{\text{in}} \approx V_{\text{out}}$, the voltage drop over the inductor is minimal, which could result in a long on-time (very low equivalent frequency).Also the secondary switch would have very short switching pulses. In hysteresis mode, a maximum on-time can be defined, or the hysteresis band should be narrowed, or a traditional scheme with exclusively $\begin{bmatrix} 1 \\ 0 \end{bmatrix}$ and $\begin{bmatrix} 0 \\ 1 \end{bmatrix}$ is used.

The hysteresis bounds should be small enough; the inductor current rising (or fall) should hit the upper and lower limit to infer the next switching action. If it fails to reach the limits, the current will oscillate to the previous hit limit, so no changes in switching action will occur, so the system will continue to oscillate, for example.

A margin of for example $m = 10\% = 0.1$ is introduced. As long as $|V_{\text{in}} - V_{\text{out}}| > (1 + m)$, the inductor voltage is regarded safe and the hereby called *Combined mode* can be used. If the voltages however lie within these

bounds, resulting in $D \approx 0.9\text{-}1.0$, in stead of reverting to an "exclusive" switching mode where $S_1 + S_2 = 1$, in PWM a *Reduced Combined PWM mode* is constructed where the duty cycles ($D1 = 1, D2 > 0.9$) are divided by the margin $(1 + m) = 1.1$ to create two duty cycles close to (but under!) 0.9, within safe bounds and with correct ratio.

If the voltages lie that far apart that a duty cycle would lie $0 < D < m$, a general disable-signal is set, which makes both duty cycles $D_1 = D_2 = 0$.

The complete range of duty cycles is demonstrated in figure 4.6

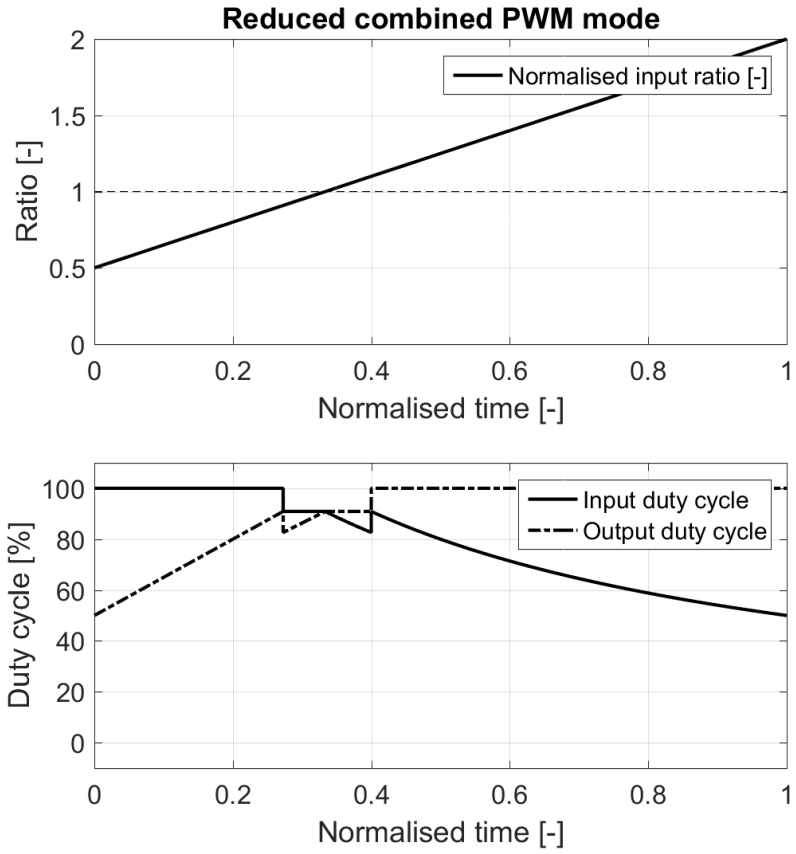

Figure 4.6: The discussed control scheme, displaying input voltage ratio (w.r.t. output voltage) and corresponding duty cycles. The Reduced combined PWM mode can be seen from 0.3 - 0.4, where the the voltages lie within 10%.

4.3.2. Hysteresis control

The hysteresis controller measures inductor current and drives the switches accordingly. The current set-point is dictated by the desired power throughput and voltage ratio between input and output. Or minimum time between switchings is 5 uS. Given an inductor of 185 µH at a maximum voltage drop with extra margin of 30 V, the current rises at $0.162\,\mathrm{A\mu s^{-1}}$. Allowing for a current ripple of ±0.162 A results in 1 µs between switching actions. Allowing for a current ripple of $\pm 0.5\,\mathrm{A_{pp}}$ results in 3.1 µs between switching actions, or an effective frequency of 161 kHz

4.4. Conclusion

The control measures the inductor current and input and output voltages and current to control the system. Both a PWM controller and a hysteresis controller were designed. In PWM, an increased (maximal) pair of duty cycles is constructed called *Combined PWM Mode*, with a reduced-mode when $V_{\mathrm{in}} \approx V_{\mathrm{out}}$. At boundaries (if either $D < 0.1$) PWM is disabled to avoid short switching pulses of transistors. At these regions, voltage ratio between input and output would be $\frac{1}{10}$, which is not likely to happen, because of the 48 V DC bus or 36 V battery - implying input voltages under 5 V and high currents, or well over 100 V. In Hysteresis control,

current boundaries are set and resulting equivalent frequencies are to be in limits.

These control methods will be simulated and tested in a prototype in coming chapters.

5

Verification: prototype

In order to verify the design of the converter and controller, a simulation was made in MATLAB and Simulink, and the design has been implemented in a prototype. The prototype was constructed both from existing hardware and from new components. This chapter revises available hardware and discussed newly designed and constructed parts.

5.0.1. Parts

In this stage the prototype is tested by the author. TU Delft has provided a bike-stand and modified e-bike to test with: from the generator of the e-bike, the leads directly to the generator output voltage terminals are available. The provided e-bike is a QWIC BASE 2, which has a three-phase PMSM mounted in the hub of the rear wheel, rated at 250 W and has a line-to-line voltage rating of approximately 0.535 $V_{p,ll}$ per rpm. It was measured to have 44 pole-pairs - which resutls in equal ratio between mechanical frequency and electrical frequency. The cranks are measured to have a radius of 17 cm. The pedalling crankshaft is connected to the rear-wheel via a gear and chain system. By means of a derailleur, several gears can be selected. The gear teeth ratios between front and rear gear are stated in table 5.1, varying from 1.57 (gear 1) to 3.14 (gear 7). The wheels are measured to have a 64 cm diameter, or a circumference of 2 m. This means that at a cycling rate of 1 Hz, an equivalent road speed of 12 $km\,h^{-1}$ to 22 $km\,h^{-1}$ is reached. The bicycle was provided with a battery model QWIC 216, a 36 V, 6 Ah Li-ion battery that can handle 144 W and has a maximum energy storage capacity of 216 Wh. At maximum power it takes 1.5 h to fully charge or discharge the battery.

Gear	Rear teeth	Gear ratio $\frac{\omega_{rear}}{\omega_{crank}}$
1	28	1.57
2	24	1.83
3	22	2.00
4	20	2.20
5	18	2.44
6	16	2.75
7	14	3.14

Table 5.1: Gearing ratios of the available bicycle. The front gear was measured to have 44 teeth.

The three-phase voltage of the PMSM is rectified and filtered to produce DC, which is converted in parallel to one or multiple batteries and grid connnections. The generated voltages vary from a rectified voltage of 20 V to 40 V DC at regular speeds (7^{th} gear, ≈1 Hz pedalling rate) to a maximum of 60 V or even 70 V at no-load. The produced energy is stored in a battery or fed back to a DC-grid. The grid connection, to remove excess energy, is simulated by an electronic load, which dissipates a set amount of current or power.

A current is drawn from a battery due to a voltage drop over the internal resistance and EMF, so the applied terminal voltage should lie close the internal back-EMF. If the voltage difference is too large, high currents could trip the fuse or damage components, leading to system failure.

5.1. Rectification

The three-phase voltage generated by the machine in the rear wheel of the stationary e-bike is then rectified to DC, in order to make it suitable for DC-DC conversion. Instead of six discrete packages with power diodes, one package with a silicon three-phase rectifier was selected advantageous, to save size without major disadvantages. It needs to block a line-to-line voltage of up to 80 V and handle up to 8 A of current, or 4 A per converter. In the workshop, a Vishay 36MT60 three-phase rectifier was readily available. This component is overdimensioned (at 600 V and 35 A), but it aids in the speed and robustness of the prototyping process. For a (cheaper) design in the future, a Vishay VS26MT20 (or comparable) suffices. This component can block up to 200 V and carry up to 25 A, enough to feed 6 converter modules maximum. The designed value of 3.2 mF was installed after the rectifier, to filter the DC voltage and currents.

5.2. Buck-boost converters

To realise the four-switch buck-boost topology as presented in Chapter 2, additional parts such as controller, power supply, mosfet drivers, voltage and current measurements, are necessary. The parts as MOSFETs and inductors need further specification. The to-be-chosen parts can be listed as:

- MOSFETs
- High and low side mosfet driver
- Inductor design
- Current measurement
- Other parts consist of generic small circuit components such as low-power resistors and small (electrolytic) capacitors.

MOSFETs

The design asks for N-type MOSFETs, capable of blocking 80 V and carrying max 4 A. To keep the overall design compact, a current rating with tolerance is advised to reduce heat in the MOSFET. The Infineon IRF630 was chosen because of the low $R_{DS(on)}$ and high current carrying capability of 9 A, or 5.7 A at high temperature. With a high $\frac{dv}{dt}$ capability, is proves suitable for fast switching application. Compared to similarly or lower priced MOSFETs, this transistor has a beneficial $R_{DS(on)}$.

High and low side mosfet driver

To drive the totempoles of MOSFETs a dedicated high and low side driver is used; the logic voltage needs to be shifted with reference to the high-side MOSFET. The International Rectifier IRS2001 was selected as it is capable of input voltages at the 3.3 V logic level of the TI microcontroller. It operates in a bootstrap mode, with a capacitor connected to the midpoint of the totempole. When the low-side transistor is on, the capacitor is charged from 12 V supply. When the high-side transistor must be turned on, this capacitor, charges to 12 V, is connected to the gate of the high-side transistor and holds this voltage difference as the midpoint "floats". A general electrolytic capacitor and fast and cheap diode (1N4148) were used.

Inductor design

From the electrical design, the peak current was found to be 4 A and a frequency of 100 kHz is according to common practices. The design of the inductors, resulting in an inductance value of 185 µH, was to wind 33 windings around two ETD29 core halves, separated by an airgap of 0.52 mm, resulting in a maximum flux density B_{max} of 300 mT. The design was realised by winding ETD29-core-halves of 3C90 material either with litz-wire and sold wire. Both wire-types fit within the winding area of the chosen core. At a diameter of 0.3 mm vs 1.0 mm, the copper wire uses a significantly smaller portion - only one layer in horizontal direction was enough. The air gap between the cores, was realised by stacking a few paper snippets, into a compressed final thickness of 0.3 mm. After LCR-measurement, the air gap width and number of turns was adjusted slightly to ensure an inductance value close to 190 µH.

Results of inductance value en series resistance LCR-measurements are summarized in table 5.2. The inductor wound from litze-wire uses nearly all of the winding area due to its larger diameter, and has half the resistance at 25 kHz.

f (kHz)	L_{solid} (µH)	L_{Litze} (µH)	R_{solid} (Ω)	R_{Litze} (Ω)
1	191.5	189.9	0.25	0.08
10	190.8	189.1	0.255	0.09
25	190.8	189.1	0.334	0.154

Table 5.2: Results of LCR-measurements of the realized inductors at 1 kHz,10 kHz and 25 kHz

Current measurement
Current measurement was implemented by a dedicated SMD chip (TI INA250). It has a 2 mΩ shunt resistor, maximal carrying 15 A. A transfer gain of $200 mV/A$ was selected, as it is the smallest gain which fits inside the 3.3 V input level of the microcontroller. A ±4 A range is projected to a ±0.4 V range around 1.6 V.

Prototype
To realize the interconnections between components, first a prototype was made on protoboard. This is a circuit board with a grid of holes and copper pads, which can be used to mount components and interconnect them. The signal routing has to be done manually and with wires. It forces the builder to have a good insight in the schematic, but the end-result can become quite cluttered - and hard to diagnose or reproduce in a possible product that spins off of this thesis. Therefore the final layout was made into a PCB design and manufactured by an external company. Results are shown in the figures 5.4. The design was made in Eagle, of which the schematic and layout are added in appendix B.

Inductors
A picture of the realised inductor is included in figure 5.3. They measure about at 3.5 x 3.5 x 2.5 cm. The completed and mounted controller and inductors are shown in figure 5.4.

Controller
The design of the PCB is centered around a TI piccolo launchpad microcontroller. These are cheap and easy-to-use microcontrollers. Simulink models, with blocks dedicated for the used microcontroller are converted to code which is run by the microcontroller. From the microcontroller, a four-signal PWM waveform with duty cycle modulation is generated, driving two high and low side drivers, each driving 2 stacked MOSFETs.

A schematic of the programmed code is shown in figure 5.2. A Reduced Combined PWM mode is implemented succesfully. The voltages are measured, processed and checked. If the input voltage is below minimum, or the voltage ratios exceed 1 : 10, the PWM-generator is disabled (set to 0 duty cycle). The microcontroller can run in “Combined” PWM mode, where one side is fully on. If the input voltage and reference output voltage lie thát close together that one of the duty cycles would become higher than 0.9, the Reduced Combined PWM mode is used: both duty cycles are divided by the margin (of 1.1) so both duty cycles are below guaranteed below 0.9. A current measurement on average input and output current is routed to the microcontroller.

5.3. Practical Waveforms

Waveforms were measured with Yokogawa current probes and Tektronics voltage probes, as available in the department at TU Delft. All measurements are displayed in pictures in the appendix A to keep the continuity of writing in this main matter.

First, the average currents around the rectifier were measured and found to be correct. Per converter, the inductor current, input current and output current were measured, along with the corresponding input or output voltage. At different load levels and power input levels, all currents are inspected and according to expectations. The current into the electronic load seems to jump, this will be due to the dynamic control of the electronic load, trying to draw the set power. The voltage output at the battery be seen oscillating, which can be due to some parasitic effects causing ringing. Handling currents up to 4 A and at varying exercise rate and intensity, the converters hold firm, no failures were experienced during testing.

5.4. Summary

In this chapter, the prototype is realised and components selected or manufactured. It has been tested to be working properly and temperature rise is within bounds. Energy transfer into and from the battery as well as into the simulated grid has been tested succesfully. The energy transfer is expected to show 5-10% losses.

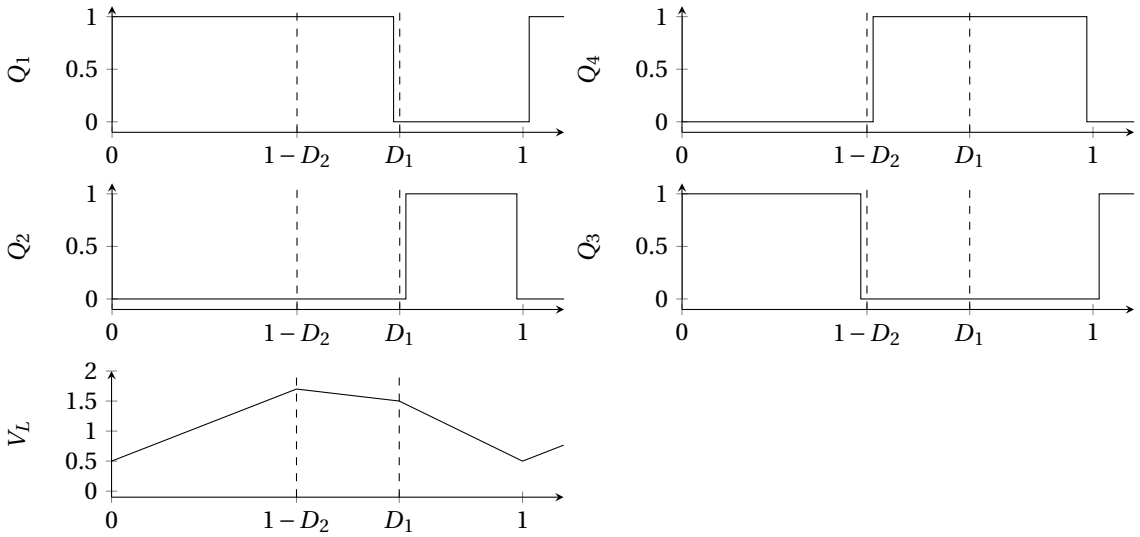

Figure 5.1: Transistor switching states and inductor voltage, with $D_1 = 0.7$ and $D_2 = 0.55$. A small deadband of 1.5% is used

Both TI controllers need 0.14 A at 3.3 V, or 1 W. The microcontroller voltage regulator draws another 2 W. Efficiency up to 85% - 90% is expected.

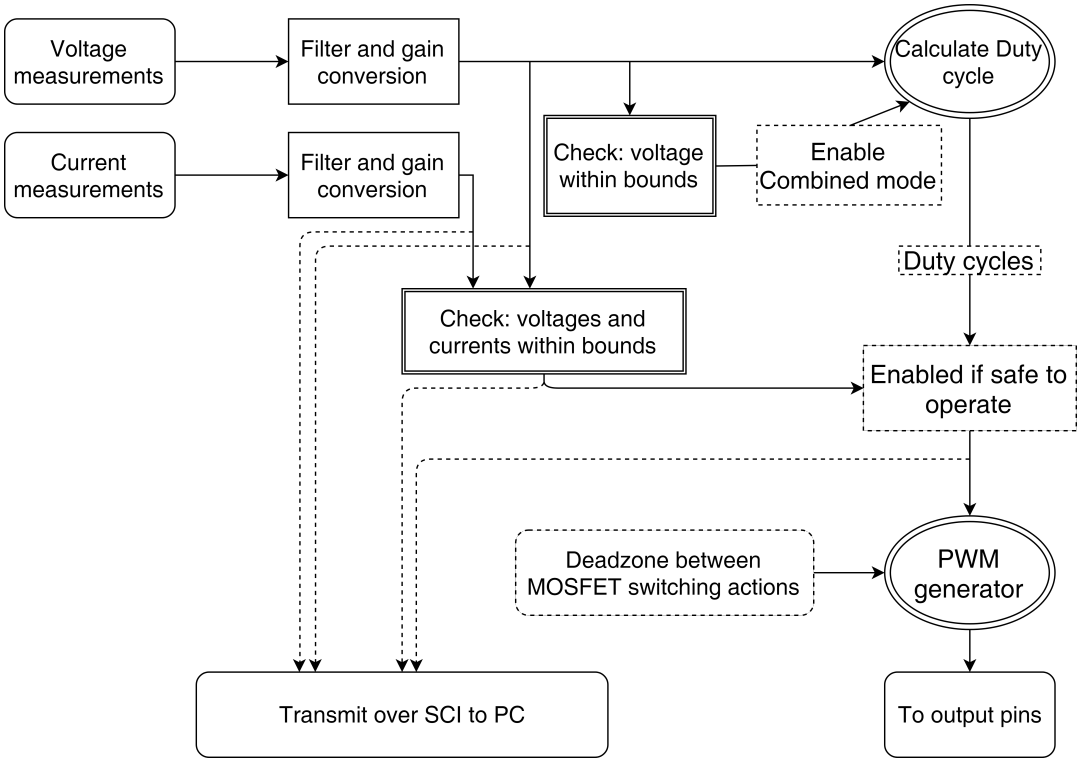

Figure 5.2: Flowchart of the code that was programmed onto the TI piccolo launchpad.

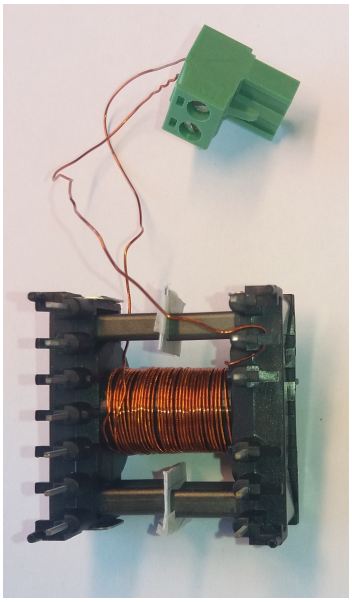

(a) The realized solid-wirewound inductor

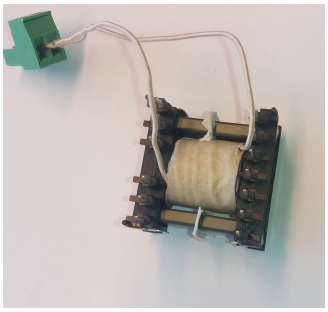

(b) The realized Litze-wound inductor

Figure 5.3: Picutres of the inductors

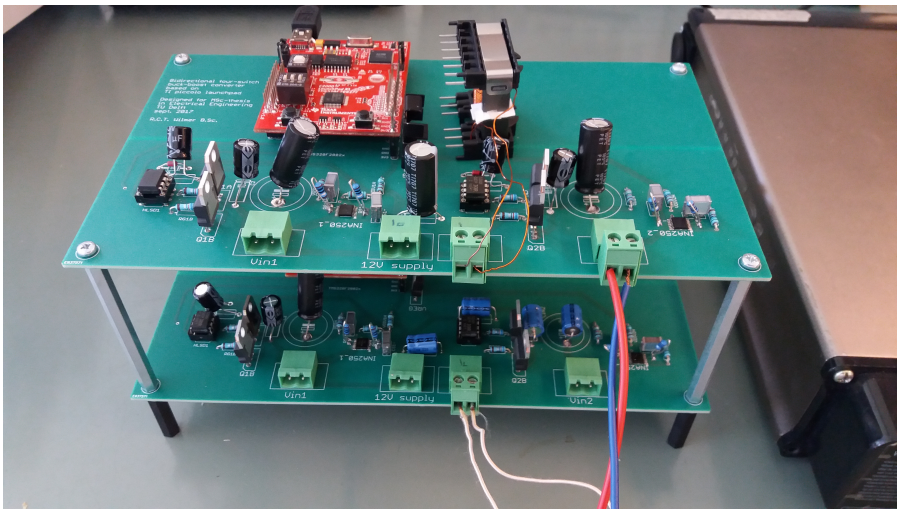

Figure 5.4: Both PCB boards mounted together. A microcontroller, inductor and the battery are visible.

6

Verification: simulations

To predict the behaviour of the designed and prototyped system, simulations were conducted by modelling the system in MATLAB and Simulink. The complete wiring of the system was modeled in Simulink, up to component level. Both a PWM and hysteresis control of two 4-switch buck-boost converters was modeled. A simulation comparing buck-boost, SEPIC and Cuk topologies was also modeled. For the peripherals, power is defined as positive when entering a load or the battery, thus negative when the battery is discharged. For the generator, a positive power means energy is transferred from the mechanical domain into the electrical converter. This chapter discusses the simulations with set-ups and outcomes. First the topologies are compared, then simulations on different scenarios with the buck-boost converter are presented.

6.0.1. Simulation parameters

To perform a detailed simulation within a reasonable time, the simulated time was held rather short at 0.04 s, or 4000 PWM periods at 100 kHz. Each simulation has different power set-points. A simulation timestep of a large value of 10 µs results in fast but inaccurate simulations. To make the timestep significantly small compared to the dynamics of the system and the PWM period, a 1 µs or even a detailed 0.01 µs per timestep can be used. The difference is illustrated in figures **??** and 6.9, where the large timestep results in oscillatory display of behaviour, which is mostly reduced at a smaller timestep of 0.1 µs or even 0.01 µs, as seen in figure **??**. If simulation settings are correct, a smaller timestep is advantageous to accuracy. If the simulation is set-up incorrectly, the simulation takes long but doesn't produce useful information. The specifications of the computer that runs the simulation bottlenecks this simulation timestep, as large simulations will require much resources, possibly hitting the limit of memory available with a system crash as a result.

6.1. Comparison to other topologies

To compare topologies, an additional simulation with Cuk and SEPIC converters was conducted. This showed that these converters, containing more storage elements in the current carrying path, have higher losses (up to 3, respectivelyt 5, times as much as buck-boost converter, as mentioned in table 3.6) and are additionally difficult to control due to the fourth-order characteristic; the voltage over the main inductor in a buck-boost converter is dependent on the input and output voltage only. In for example a Cuk controller, the capacitor current depends on the inductor currents, of which the voltages depend on the history of the capacitor current. A small error, if amplified, might result in large effects on the whole system.

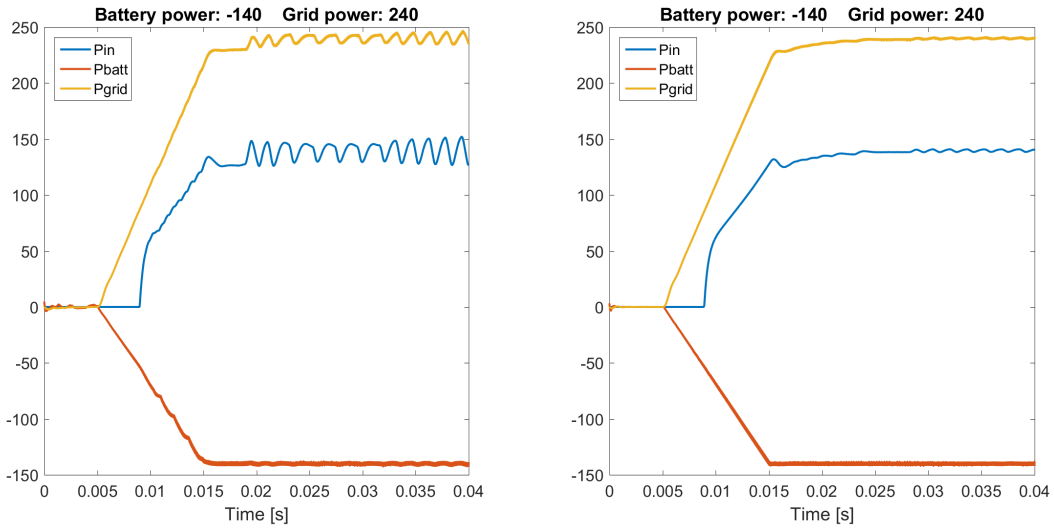

(a) A simulation conducted with a large timestep of 1 µs, (b) A simulation conducted with a small timestep of 10 ns resulting in inaccurate simulation results

Figure 6.1: Comparison of power flows in a simulation of a three-port converter, at different timesteps. P_{in} denoting mechanical input power

6.2. Double bidirectional four-switch buck-boost converter

The three-port topology is realised by a capacitor bank which collects energy from the stationary e-bike generator rectifier, connected to two buck-boost converters. The buck-boost converter connected to the battery has a bidirectional current capability, in order to both store and retrieve energy from the battery.

6.3. Simulation settings

Different set-point are used for the simulations. From standstill, the bike accelerates to operating speed at highest gear. Hereafter, the load power is increased to operating point. The different power scenarios were chosen:

- From the bicycle into the battery: 140 W
- From the bicycle directly into the grid: 100 W
- From battery fed-back into a grid connection, 140 W
- From the bicycle both into the battery and the grid, 100 W + 140 W.

The system is investigated in steps, first only the generator and rectifier were modeled, both in an unloaded and a loaded scenario. Then the converters are added to present the full three-port topology.

6.3.1. Settings

The user is modelled by PI-controlling a torque as the input to the PMSM machine, based on the speed error. A minimum torque of 0 N m is set (no braking) and a maximum corresponding to 50 kg on 17 cm cranks with gear ratio 3.14 to the rear wheel. The simulation starts at standstill of the machine, accelerating linearly up to rated speed. To represent the real-world parts as closely as possible, the equivalent component values were measured or calculated, and are stated in table 6.1. These values are used in models presented by the MATLAB Simulink environment.

In figure 6.3, the unloaded rectifier is shown. The electrical period of the generator at a typical frequency of 3.14 Hz of the rear wheel is 1.2 ms. The voltage drop over the rectifier diodes can be seen, as well as the six-pulse characteristic which is inherit to the three-phase rectifier topology.

When the rectifier is being loaded, as in figure 6.4, the phases show a commutation period, and a conducting period where the terminal voltage of the generator equals the capacitor voltage. Both are reason for

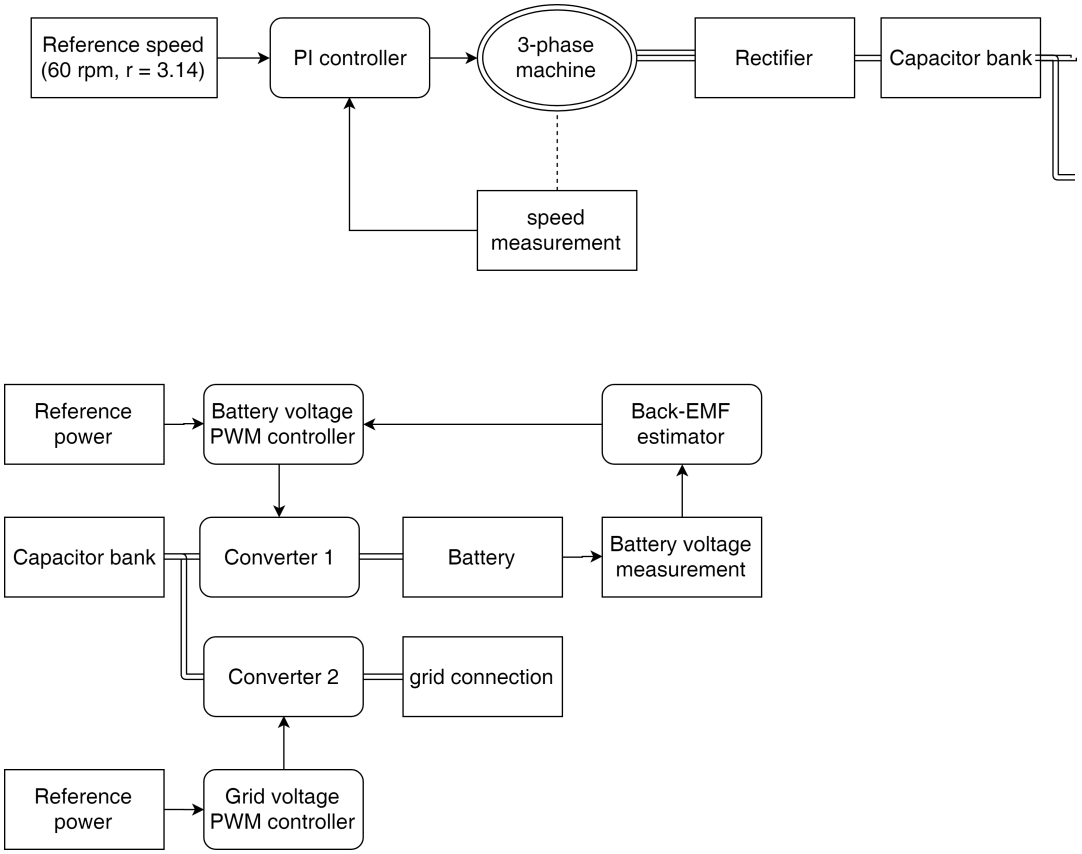

Figure 6.2: Flowchart of the code that simulates the electrical system. The figure is split in half; the capacitor bank is displayed in duplicate.

the “indents” in the sinusoidal shape. In figure 6.5, a phase current is displayed. The rectifier current has both an average value, which flows into a load resistor, and an AC part that flows in the capacitor. The resistor is fed from the (constant) capacitor voltage. Of the complete six-phase cycle, the phase current is positive for two pulses, one pulse zero, and two pulses negative output current (and one pulse zero again). This is due to which diode pair is conducting, which results from which line-to-line voltage is greatest in amplitude.

Machine		
Three-phase permanent magnet synchronous machine		
Moment of intertia J	0.17	$\mathrm{kg\,m^2}$
Number of pole-pairs p	44	–
Machine constant K_V	0.535	$\mathrm{V\,rpm^{-1}}$
Phase inductance L_s	360	µH
Phase resistance R_s	0.14	Ω
Rectifier		
Forward voltage V_f	0.7	V
On-resistance R_{on}	0.05	Ω
Converter		
Inductor L	190	µH
Equivalent series resistance R	0.2	Ω
Input and output filter capacitors C	100	µF
MOSFETs		
On-state resistance R_{on}	0.35	Ω
Internal body-diode resistance R_d	0.025	Ω
Internal body-diode forward voltage drop V_f	0.73	V
Battery		
Nominal battery voltage	36	V
Capacity	6	Ah
Fully charged battery voltage	40.5	V
Nominal discharge current	2.34	A
Internal resistance R_{int}	0.71	Ω

Table 6.1: Measured and simulated characteristics

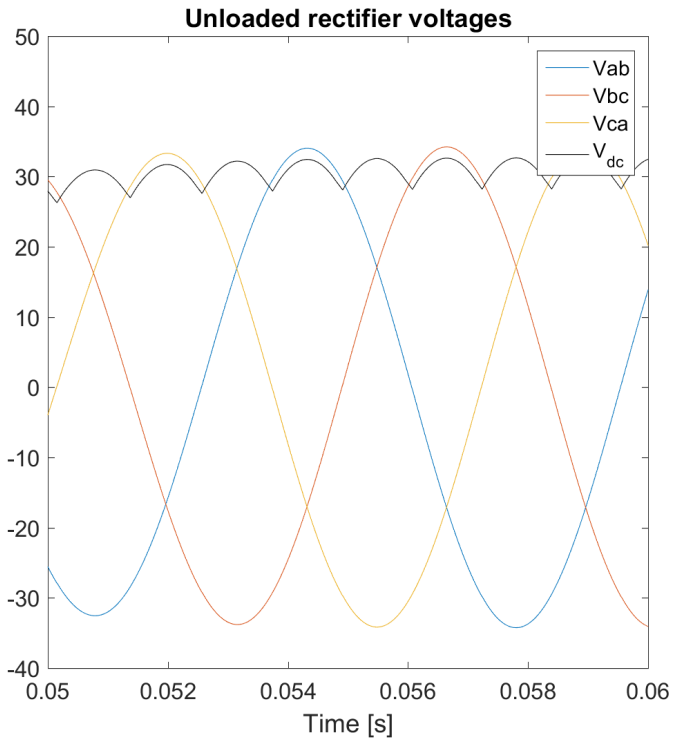

Figure 6.3: Simulation result of unloaded rectifier. Measuring generator terminal line-to-line voltages, and rectified voltage V_{dc}.

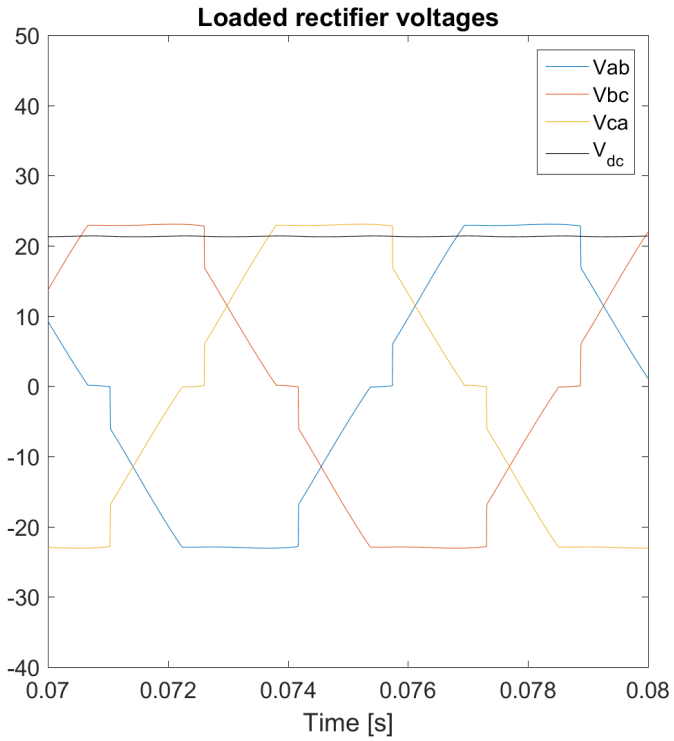

Figure 6.4: Simulation result of loaded rectifier. The capacitor voltage lies under the peak generator voltage: when the diodes conduct, the sinusoid has a flat top

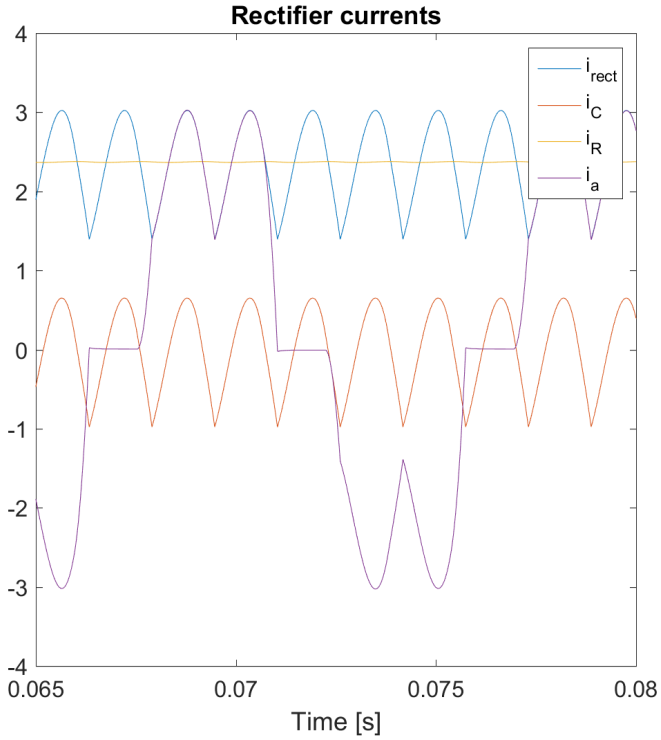

Figure 6.5: Simulation result of rectifier currents. The capacitor filters the AC part of the output current, the resistor is fed by a constant voltage. One phase current is displayed, indicating both positive and negative conducting states, as well as the commutation and zero period. i_{rect} denoted rectifier output current, feeding the capacitor with i_C a parallel resistor i_R. i_a denotes one generator phase current.

These simulations are according to expected theory, so the converters were added and simulated. First the bike is cycled up to speed, then the battery power and grid power are introduced. The average powers closely follow set point from the time they were turned on. It turned out that the simulation timestep should be small to provide accurate simulations. The system does not show any instability from these changes in set-points.

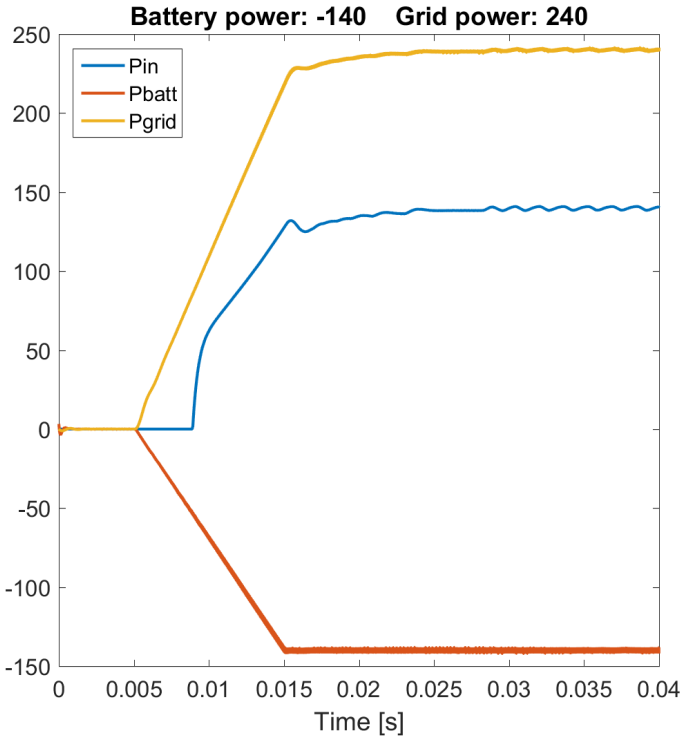

Figure 6.6: Simulation result of three-port topology, with very fine timestep (10 ns). The power flows purely into the battery. Y-axis is off course measured in W.

6.4. Full three-port simulation

In this simulation a 4-switch buck-boost converter is controlled in combined duty-cycle control to feed into the battery. From the referene power, reference output voltage is calculated. In the controller, the duty cycles are calculated as in equations (6.1)-(6.2).

$$D_1 = \max\left(1, \frac{V_{out,ref}}{V_{in}}\right) \tag{6.1}$$

$$D_2 = \frac{V_{in}}{V_{out,ref}} \cdot D_1 \tag{6.2}$$

The power set points (100 W into battery, 100 W into grid, and 140 W+100 W into the grid) are followed accordingly. A small percentage of the power is lost.

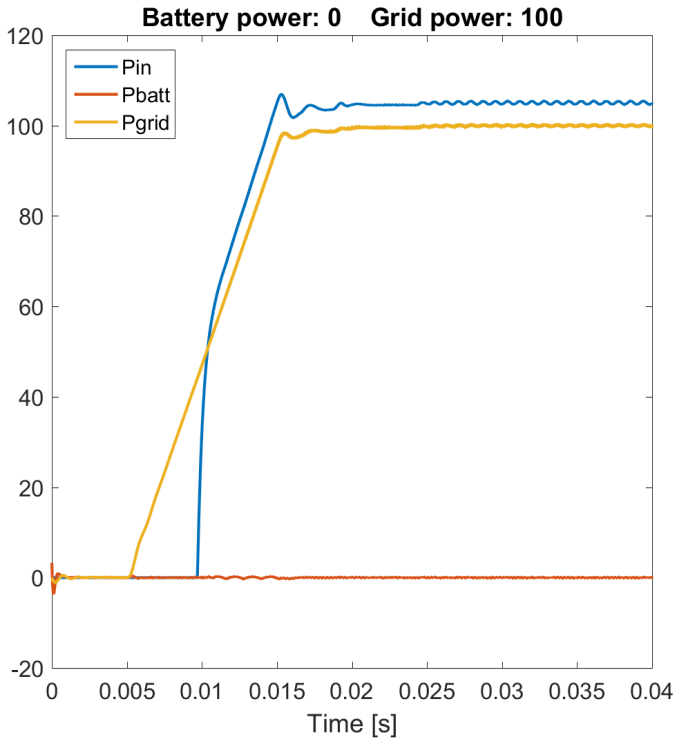

Figure 6.7: Simulation result of three-port topology, with very fine timestep (10 ns). The power flows purely into the grid. Y-axis is off course measured in W.

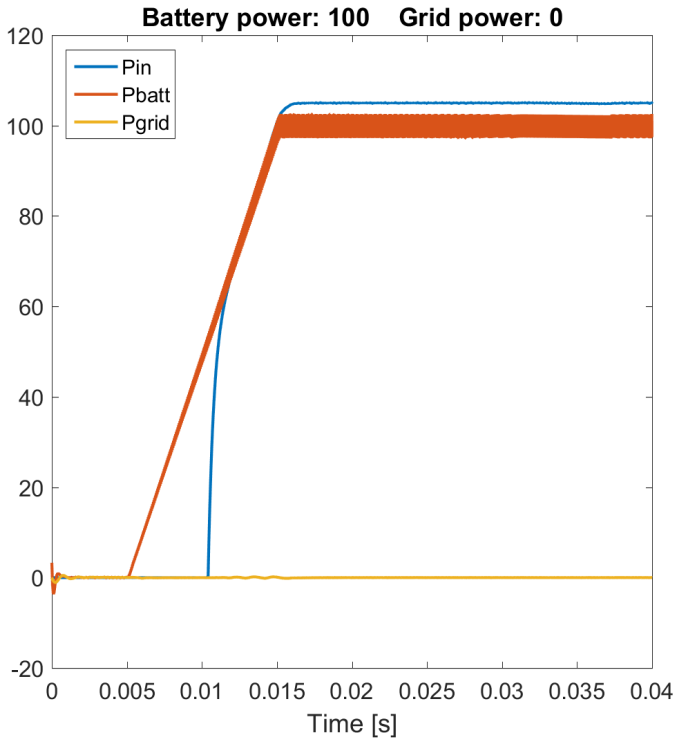

Figure 6.8: Simulation result of the three-port topology, with very fine timestep (10 ns). The generated power flows into the grid, and the battery is discharged at 140 W. Y-axis is off course measured in W.

6.5. Comparing Topologies

To compare Cuk, buck-boost and SEPIC topologies, a simulation was run with three parallel converters, fed by a PMSM-model and connected to a capacitor and burn-resistor as load.

The main reason for this simulation was to investigate the power losses, which increase by a factor of 3 for the SEPIC or even 5 for the Cuk converter. This has been summarised in table 3.6. Therefore, a buck-boost converter seems preferable for this application.

The input and output currents are displayed, of which the buck-boost input current and the SEPIC output current are measured to be discontinuous, needing a relatively large filter capacitor.

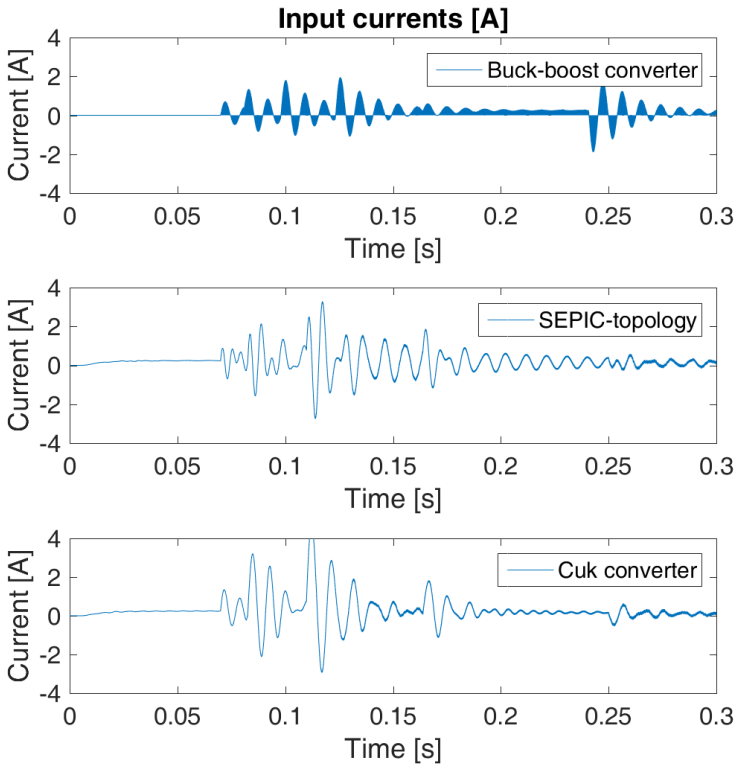

(a) Comparative input currents

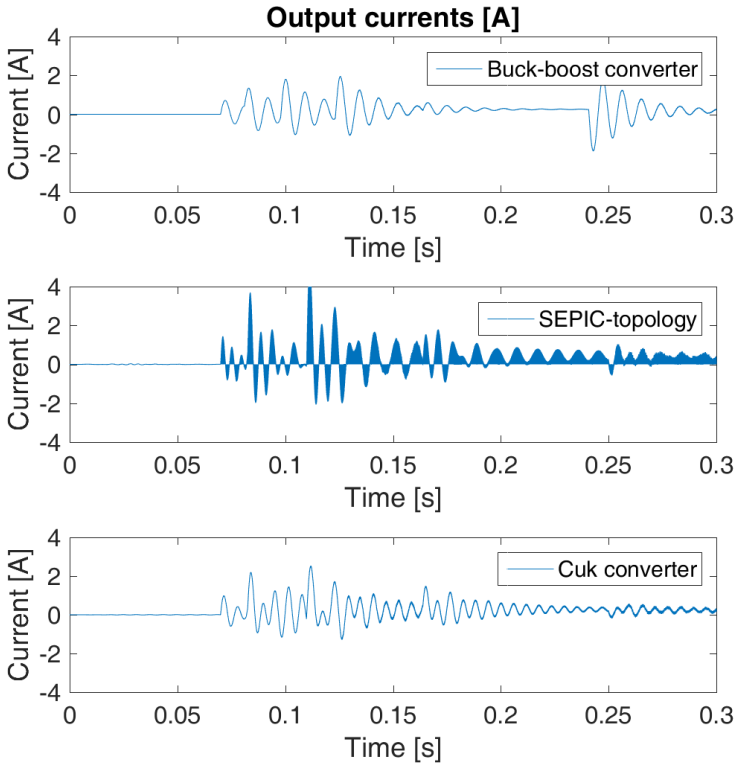

(b) Comparative output currents

Figure 6.9: Comparison of simulations with different timesteps. Displayed are the buck-boost, SEPIC and Ćuk converter topologies from top to bottom. A part of the simulation, from 0 s to 0.3 s was chosen.

6.6. Summary

Detailed simulations of the system consisting of generator, rectifier, converters and load were conducted. A comparison between topologies (buck-boost, SEPIC or Ćuk) and a comparison between control modes (PWM, hysteretic with L-filter current sensor, Combined PWM mode and Reduced Combined PWM mode) were conducted. The buck-boost topology deemed most promising and efficient. A PWM controller is easy to implement and doesn't rely on a good current measurement. Both Combined and Reduced Combined PWM mode were tested successfully, keeping the system in a safe operating area. Different scenario's of power levels were introduced: ± 140 W into (and from) the battery, and a power level of 100 W from the generator, resulting in a maximum of 240 W into the grid. Decreasing the simulation timestep aids to accuracy of the simulation. Energy transfer into and from the battery as well as into the simulated grid has been tested.

In simulations a typical buck-boost behaviour was shown. Although a fast load switch of zero to typical load in 0.01 s (at full torque of the user), the converters have no trouble following this set point. The controller is shown to be stable in the applied and simulated conditions.

7

Conclusion and recommendations

This final chapter concludes the thesis. It reflects on the results and research questions, as well as posing recommendations for future work. To construct a platform that promotes health and energy awareness, a prototype human power generator has been designed, simulated and realised. Overal, the process of realising a converter has been described. The models are useful for estimation. The prototype works and can demonstrate the envisioned platform - which aids in human health and energy awareness.

7.1. Reflecting on results

Per chapter, a summary is presented. In chapter 1, the project and the system have been explained. In chapter 2 was filled with theory on human power, mechanical interaction, electromechanical conversion, electrical conversion, storage and load. Magnetics and magnetic circuit theory was presented. In chapter 3, the actual design was made. An eletrical system of a three-phase PMSM, rectifier and two buck-boost converters is proposed, along with detailed values. In chapter 4 the control is designed. Both hysteresis and PWM mode are proposed. PWM mode has been enhanced with theory on the Combined PWM Mode, as well as a Reduced Combined PWM mode. Current measurement tactics were discussed. In chapter 5 a prototype is realised. Components were selected and the microcontroller programmed. The inductors are made. A PCB has been designed and ordered at an external company. From the working prototype waveforms - which are presented in the appendix - are measured and discussed. In chapter 6 the complete system, with component values as implemented in the prototype, is simulated. Simulation settings, influences and flowchart are given. Simulated waveforms are discussed and the simulation is found to be accurate to reality. The prototype was realised with hardware from the TU Delft and by designing and building two inductors and two PCBs. It was succesfully tested and still is operational.

7.2. Research questions

Research questions aid in structuring the research and providing conclusions. The research questions are answered throughout the thesis. The objectives are:

- Propose a three-port converter for efficient conversion of energy on a stationary e-bike with battery connected to a 48 V DC bus
- Design a controller which ensures the efficient conversion and constant (w.r.t. angle of rotation) torque on the rear wheel, just like riding a bike on the road.
- Validate the result through construction of a user prototype

And the results were shown:

- The converter has been proposed in detail, to be used between e-bike, battery and a 48 V DC bus. It uses a three-port DC-DC converter topology that consists of two buck-boost converters, of which one has bidirectional current capabilities.

- The control scheme of both a hysteresis controller and a PWM controller have been proposed and simulated. An additional Combined PWM mode and Reduced Combined PWM mode have been proposed. All three PWM modes proved to work in the prototype. The experienced torque has been categorised as stable per rotation, but between rotations at different speeds, it could differ.
- The prototype is built and has proven in tested situations, handling current and power levels as designed.

7.3. Electrical

From the input restrictions, a working system is designed and built. The used components are quite cheap solutions which still fit to ratings. Some over-dimensioning even happened, due to manufacturers not making smaller components, or which didn't cost significantly less.

7.3.1. Three-port converter

From the input to storage and grid-connection, a double bidirectional buck-boost converter is proposed with ratings according to load and input specifications.

7.3.2. Controller

The controller that was designed controls the inductor current, to accurately and dynamically control the system. In real-life, current measurement was difficult to obtain, so a PWM-control scheme was firstly implemented to ensure proper working of all hardware and safe operating area to the external components such as battery.

7.3.3. Prototype

On the realised prototype, waveforms have measured the electrical system and the converter to behave appropiate. Both combined and reduced combined PWM mode have been shown to work. The user cycled for some varying speeds and powers, and different grid currents settings were tried, all at a stable system.

7.4. Future recommendations

To improve the system even further, an investigation into better hardware could be made, with a better voltage and current measurement. If a fast current measurement can be accomplished, a Cuk converter topology in BCM could be accomplished. A faster controller also implies a more stable system.

To help in stimulating the user, an app can be developed in which a display not only shows settings, but also compares the produced energy to, for example; the energy a human needs to burn after eating a candy bar, or the electricity is compared to the equivalent energy needed to make one cup of coffee.

A

Practical waveforms

In this chapter, pictures are shown that demonstrate the functioning of the converters.

A.1. Average currents to and from DC bus

Three currents were measured: rectifier current, battery current and grid (load) current. First, the battery is discharged into the load. Normal behaviour is seen at both 1.0 A and 1.6 current levels. Then, the bicycle is measured to produce 3.39 A which flows both into the bicycle 2.7 A and into the grid 0.7 A. This confirms the average working of the converters. It is suspected Kirchhoff's current law still holds.

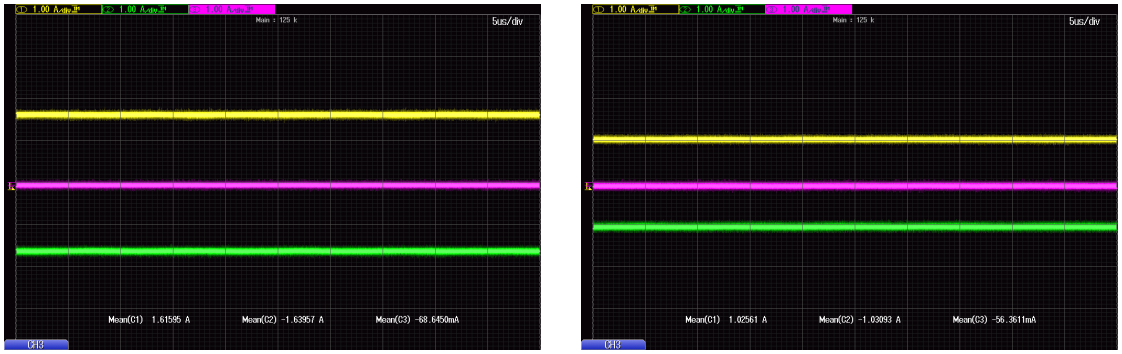

(a) Battery discharging 1.6 A into an electronic load via two converters

(b) Battery discharging 1.0 A into an electronic load via two converters

Figure A.1: Current measurement of Battery into Grid operation

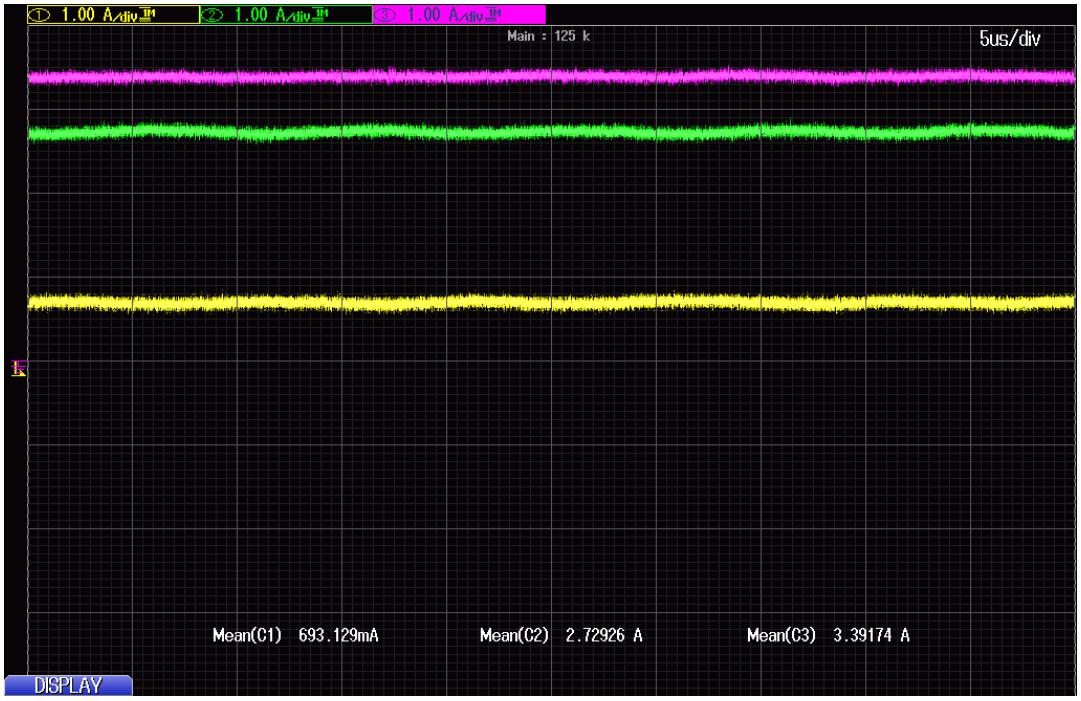

Figure A.2: Current measurement of Bicycle being operated, delivering current to both the Battery and the Grid.

A.2. Converter: Inductor currents

Next, the battery converter is investigated. The inductor current is measured, as well as input and output currents, and the DC-bus voltage. First idle, then the battery feeds into a grid load of 0.6 A. At last, the bicycle feeds into the grid.

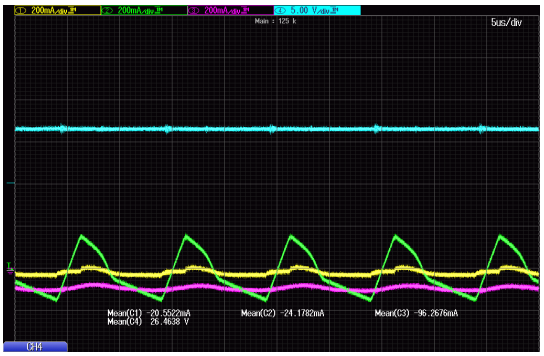

(a) Small operation / idle

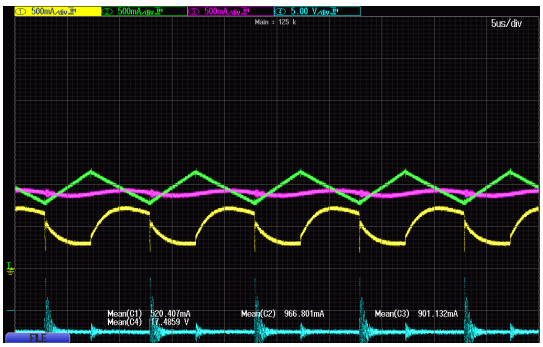

(b) The electronic load increased to about 0.6 A

Figure A.3: Current measurement of Battery into Grid operation

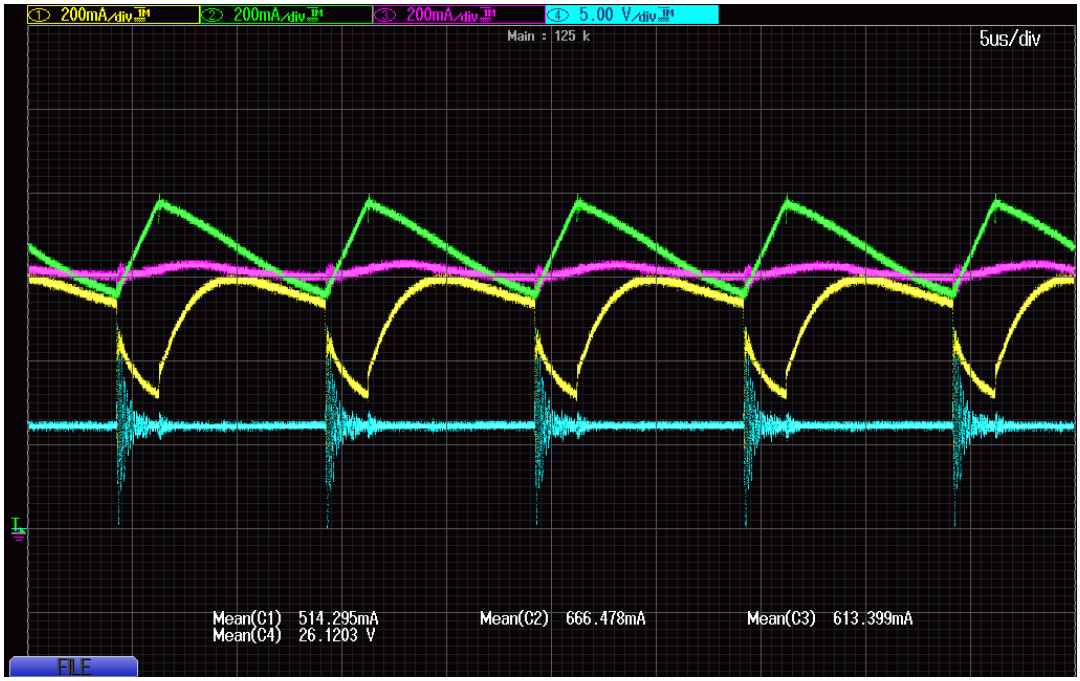

Figure A.4: The generator loads into both the bicycle and the load.

A.3. Both converters

Next, the power generated by the user is varied. It is tested at current levels (set at the electronic load) of both 0.2 A and 0.6 A. The inductor current behaves properly. The oscilloscope was set to AC couple this current, so the mean current value reading of Ch2 (the inductor current) is inaccurate. It is seen that average current are not equal, but according to voltage ratios, as expected from theory.

In figure A.6 (current coupling is set to DC again), the influence of the two parallel converters can be seen on the DC bus voltage, giving rise to ringing. The currents are behaved.

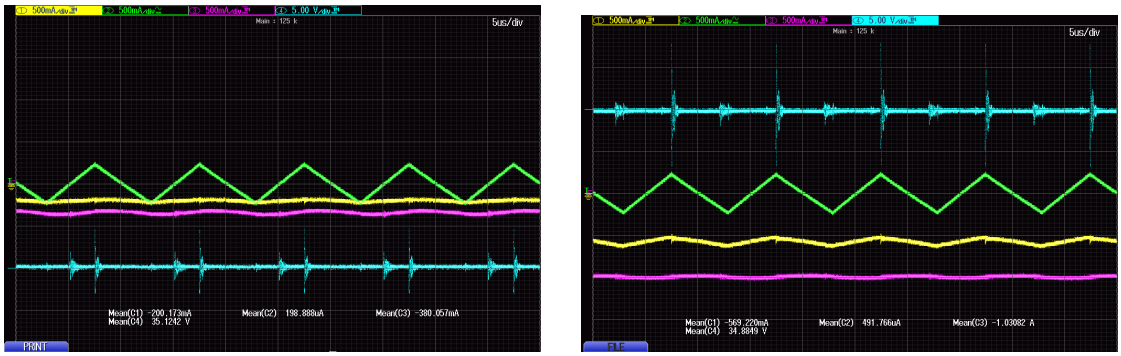

(a) Low loaded bicycle

(b) Higher load

Figure A.5: Current measurement of Battery into Grid operation

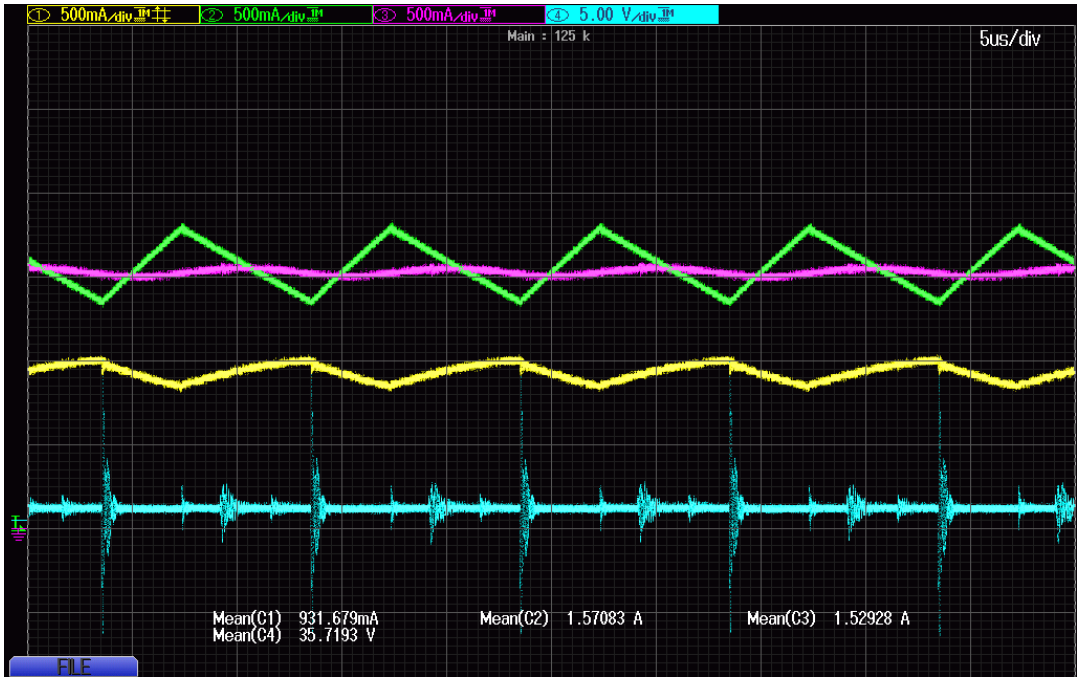

Figure A.6: DC Inductor current, battery voltage

A.4. Double converter; voltage ripples

Next, two currents and two voltages are measured. Both battery to grid conversion and bicycle to load conversion have been verified. In figure A.7b, the double ripple is seen as the bicycle converter also kicks in.

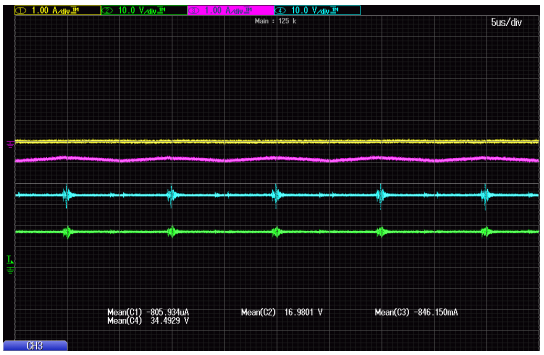

(a) A load of 0.8 A fed from battery

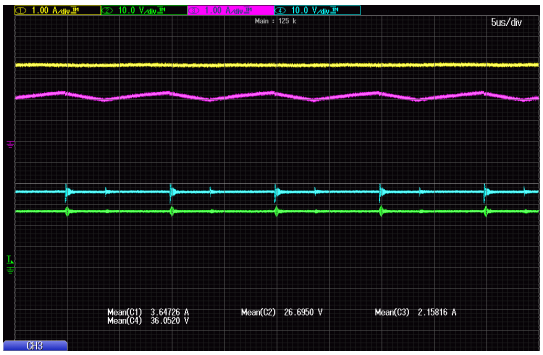

(b) Bicycle and a 1.5 A load

Figure A.7: Current measurement of Battery into Grid operation

B

PCB Layout

In this chapter, the layout of the designed PCB is presented. The ground plane is separated in two planes with a small connection, to separate the analogue measurement at the microcontroller from the switching converter with possible interference. It is not depicted here.

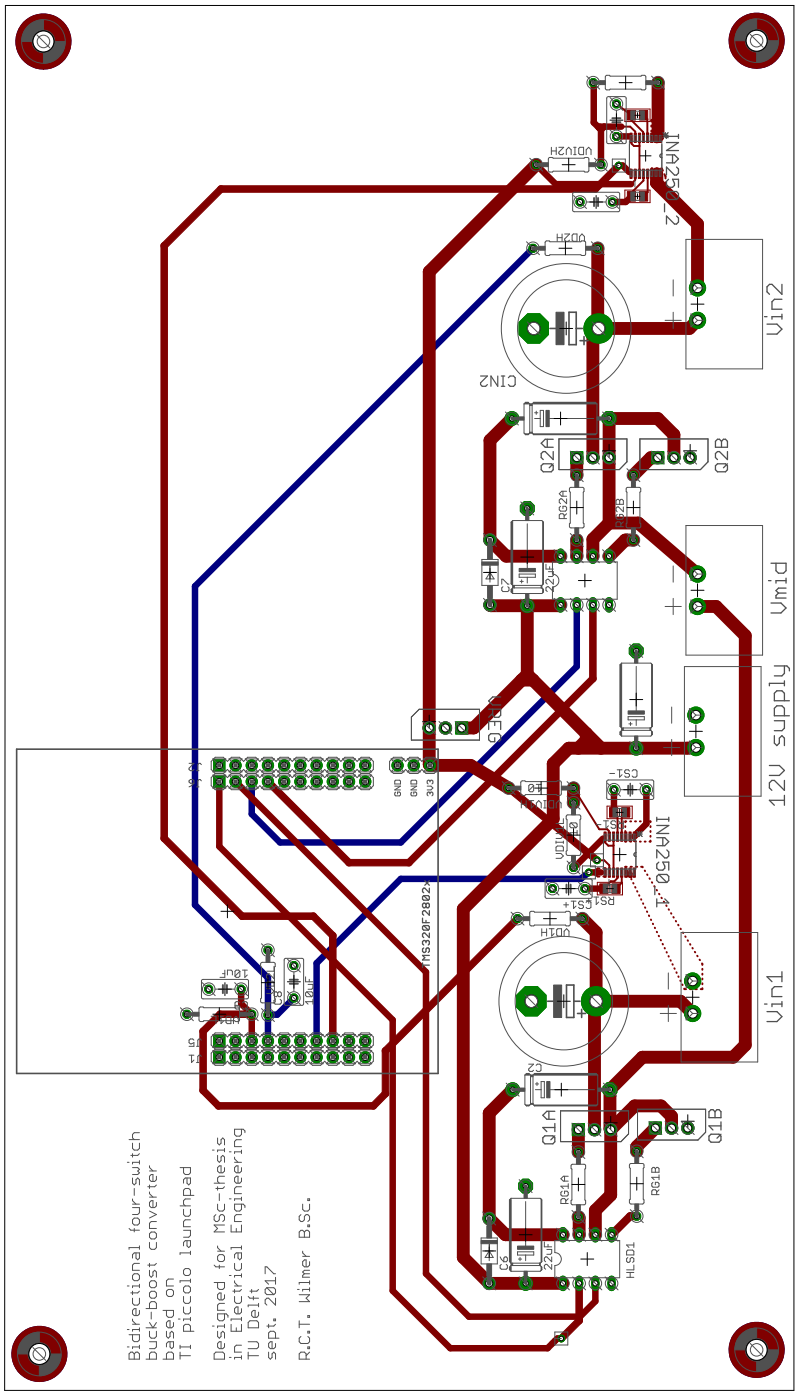

12-8-2017 10:09 f=1.25 C:\Users\Rik\Documents\eagle\BidiBuckBoost\BBB_final.brd

Bibliography

[1] K. c. Bae, S. c. Choi, J. h. Kim, C. y. Won, and Y. c. Jung. Lifepo4 dynamic battery modeling for battery simulator. In *2014 IEEE International Conference on Industrial Technology (ICIT)*, pages 354–358, Feb 2014. doi: 10.1109/ICIT.2014.6894892.

[2] Ph.D. Chester R. Kyle and Frank Berto. The mechanical efficiency of bicycle derailleur and hub-gear transmissions. *Human power*, (52):3–11, 2001. ISSN 0898-6908. URL http://www.ihpva.org/HParchive/PDF/hp52-2001.pdf.

[3] S. Cuk and R. D. Middlebrook. A new optimum topology switching dc-to-dc converter. In *1977 IEEE Power Electronics Specialists Conference*, pages 160–179, June 1977. doi: 10.1109/PESC.1977.7070814.

[4] Tamara Dean. *The Human-Powered Home*. New Society Publishers, 2008. URL http://www.ebook.de/de/product/7380924/tamara_dean_the_human_powered_home.html.

[5] Diabetesfonds. Diabetes in cijfers, 2015. URL https://www.diabetesfonds.nl/over-diabetes/diabetes-in-het-algemeen/diabetes-in-cijfers.

[6] Jeff Falin. Applicaton note slyt372: Designing dc/dc converters based on zeta topology, 2010.

[7] H. P. Forghani-zadeh and G. A. Rincon-Mora. Current-sensing techniques for dc-dc converters. In *The 2002 45th Midwest Symposium on Circuits and Systems, 2002. MWSCAS-2002.*, volume 2, pages II–577–II–580 vol.2, Aug 2002. doi: 10.1109/MWSCAS.2002.1186927.

[8] Xiaosong Hu, Shengbo Li, and Huei Peng. A comparative study of equivalent circuit models for li-ion batteries. *Journal of Power Sources*, 198:359 – 367, 2012. ISSN 0378-7753. doi: http://dx.doi.org/10.1016/j.jpowsour.2011.10.013. URL http://www.sciencedirect.com/science/article/pii/S0378775311019628.

[9] W. G. Hurley and W. H. Wölfle. *Transformers and Inductors for Power Electronics*. John Wiley & Sons, 2013. ISBN 9781118544679. URL http://www.ebook.de/de/product/21167490/w_g_hurley_w_h_woelfle_transformers_and_inductors_for_power_electronics.html.

[10] A. A. H. Hussein and I. Batarseh. An overview of generic battery models. In *2011 IEEE Power and Energy Society General Meeting*, pages 1–6, July 2011. doi: 10.1109/PES.2011.6039674.

[11] A. "Jansen and P." Slob. Human Power; Comfortable One-hand Cranking. In *International Conference on Engineering Desing (ICED), Stockholm*, August 2003.

[12] A. J. Jansen and A. L. N. Stevels. Human power, a sustainable option for electronics. In *Electronics and the Environment, 1999. ISEE -1999. Proceedings of the 1999 IEEE International Symposium on*, pages 215–218, 1999. doi: 10.1109/ISEE.1999.765878.

[13] Marian K. Kazimierczuk. *High-Frequency Magnetic Components*. Imprint unknown, 2011. ISBN 1119964911. URL https://www.amazon.com/High-Frequency-Magnetic-Components-Marian-Kazimierczuk/dp/1119964911?SubscriptionId=0JYN1NVW651KCA56C102&tag=techkie-20&linkCode=xm2&camp=2025&creative=165953&creativeASIN=1119964911.

[14] LINFINITY. Application note an-7: A simple current-sense technique eliminating a sense resistor. Copyright © 1998 Rev 1.1 07/98.

[15] Colonel Wm T. McLyman. *Transformer and Inductor Design Handbook (Electrical Engineering & Electronics)*. Taylor & Francis Inc, 2004. ISBN 9780824751159. URL https://www.amazon.com/Transformer-Inductor-Electrical-Engineering-Electronics/dp/0824751159?SubscriptionId=0JYN1NVW651KCA56C102&tag=techkie-20&linkCode=xm2&camp=2025&creative=165953&creativeASIN=0824751159.

[16] Méndez-Gayol, M. Rico-Secades, M. Calleja, A. J. Pablo, and J. Quintana. Working in a smart grid for a sustainable gym. In *2016 13th International Conference on Power Electronics (CIEP)*, pages 289–294, June 2016. doi: 10.1109/CIEP.2016.7530772.

[17] N. Mohan, T. Undeland, and W. Robbins. *Power Electronics - Converter, Applicatons and Design (3rd Ed.)*. Wiley, 3 edition, 2003. ISBN 978-0-471-22693-2.

[18] R. H. "Morton and D. J." Hodgson. The relationship between power output and endurance: a brief review. *European Journal of Applied Physiology and Occupational Physiology*, 73(6):491–502, 1996. ISSN 1439-6327. doi: 10.1007/BF00357670. URL http://dx.doi.org/10.1007/BF00357670.

[19] A. M. Patel and M. Ferdowsi. Advanced current sensing techniques for power electronic converters. In *2007 IEEE Vehicle Power and Propulsion Conference*, pages 524–530, Sept 2007. doi: 10.1109/VPPC.2007.4544180.

[20] J. J. H. "Paulides, J. W. Jansen, L. Encica, E. A. Lomonova, and M." Smit. Human-powered small-scale generation system for a sustainable dance club. In *Electric Machines and Drives Conference, 2009. IEMDC '09. IEEE International*, pages 439–444, May 2009. doi: 10.1109/IEMDC.2009.5075243.

[21] R. A. Prakoso. Extra project: Human powered generator, 2016.

[22] M. Rosu-Hamzescu, S. Oprea, and Microchip Technology Inc. High-power cc/cv battery charger using an inverse sepic (zeta) topology, 2012.

[23] P.C. Sen. *Principles of Electric Machines and Power Electronics*. Wiley, 2nd edition, 1996. ISBN 9971-51-204-1. URL https://www.amazon.com/Principles-Electric-Machines-Power-Electronics/dp/9971512041?SubscriptionId=0JYN1NVW651KCA56C102&tag=techkie-20&linkCode=xm2&camp=2025&creative=165953&creativeASIN=9971512041.

[24] Daniel Torres. Comparing motor-control techniques. *Electronic Component News*, 2009. URL https://www.ecnmag.com/article/2009/10/comparing-motor-control-techniques.

[25] Georgios A. Villias. Design of the Human-Powered Generator Module of the Renewable Energy Sharetech Hybrid System. Master's thesis, Delft University of Technology, March 2013.

[26] J. Wu, C. Zhang, and Z. Chen. A novel lithium-ion battery model for state of charge estimation under dynamic currents. In *2015 4th International Conference on Electric Power and Energy Conversion Systems (EPECS)*, pages 1–6, Nov 2015. doi: 10.1109/EPECS.2015.7368513.